



CENTER FOR HYPERSONIC COMBINED CYCLE FLOW PHYSICS

James Mcdaniel
UNIVERSITY OF VIRGINIA

03/24/2015
Final Report

DISTRIBUTION A: Distribution approved for public release.

Air Force Research Laboratory
AF Office Of Scientific Research (AFOSR)/ RTA1
Arlington, Virginia 22203
Air Force Materiel Command

| | | | | | |
|--|-------------|-------------------------|-------------------------------|---|---|
| REPORT DOCUMENTATION PAGE | | | | Form Approved OMB No. 0704-0188 | |
| <p>The public reporting burden for this collection of information is estimated to average 1 hour per response, including the time for reviewing instructions, searching existing data sources, gathering and maintaining the data needed, and completing and reviewing the collection of information. Send comments regarding this burden estimate or any other aspect of this collection of information, including suggestions for reducing the burden, to the Department of Defense, Executive Service Directorate (0704-0188). Respondents should be aware that notwithstanding any other provision of law, no person shall be subject to any penalty for failing to comply with a collection of information if it does not display a currently valid OMB control number.</p> <p>PLEASE DO NOT RETURN YOUR FORM TO THE ABOVE ORGANIZATION.</p> | | | | | |
| 1. REPORT DATE (DD-MM-YYYY) 23-03-2015 | | 2. REPORT TYPE Final | | 3. DATES COVERED (From - To) 06/01/2009 - 12/31/2014 | |
| 4. TITLE AND SUBTITLE CENTER FOR HYPERSONIC COMBINED CYCLE FLOW PHYSICS | | | | 5a. CONTRACT NUMBER | |
| | | | | 5b. GRANT NUMBER FA9550-09-1-0611 | |
| | | | | 5c. PROGRAM ELEMENT NUMBER | |
| 6. AUTHOR(S) McDaniel, James C., Jr. Edwards, Jack R, Jr. Cutler, Andrew D. Chelliah, Harsha K. Goynne, Christopher P. | | | | 5d. PROJECT NUMBER | |
| | | | | 5e. TASK NUMBER | |
| | | | | 5f. WORK UNIT NUMBER | |
| 7. PERFORMING ORGANIZATION NAME(S) AND ADDRESS(ES) University of Virginia, Dept. of Mechanical and Aerospace Engineering, Charlottesville, Va North Carolina State University, Dept. of Aerospace Engineering, Rayleigh, NC George Washington University, Dept. of Mechanical Engineering, Arlington, VA | | | | 8. PERFORMING ORGANIZATION REPORT NUMBER FA9550-09-1-0611 | |
| 9. SPONSORING/MONITORING AGENCY NAME(S) AND ADDRESS(ES) Air Force Office of Scientific Research 875 N Randolph St Room 3112 Arlington, VA 22203 | | | | 10. SPONSOR/MONITOR'S ACRONYM(S) AFOSR | |
| | | | | 11. SPONSOR/MONITOR'S REPORT NUMBER(S) | |
| 12. DISTRIBUTION/AVAILABILITY STATEMENT Approved for Public Release | | | | | |
| 13. SUPPLEMENTARY NOTES | | | | | |
| 14. ABSTRACT Combined cycle flow physics were investigated using a team of expert experimentalists and numerical and chemical kinetic modelers. Flowfields were examined in the turbine/ramjet dual inlet mode transition using data from the NASA Glenn IMX facility and RANS calculations. In the ramjet/scramjet mode regime a dual-mode combustion wind tunnel was developed at the University of Virginia for extensive data acquisition using various techniques, including OH PLIF, CARS, TDLAS, TDLAT and SPIV. It was established that the flow operated in the dual-mode at high equivalence ratios due to a pre-combustion shock train, but was supersonic at low equivalence ratios. The NASA HyPulse facility at ATK/GASL was utilized for testing at Mach 7 and 10. RANS models of the dual-mode flowfield produced results that were very well compared to experimental data. FDF models were developed to demonstrate the advantage of particle-based approaches. Chemical kinetic model reduction strategies were developed to reduce the number of specie required. The flame angle from a cavity flame holder was well predicted by classical turbulent flame-speed estimates in a well-premixed cavity-stabilized flowfield, established using a precombustion shock train. | | | | | |
| 15. SUBJECT TERMS Hypersonic combined cycle propulsion, turbine/ram dual-inlet transition, ram/scram dual-mode transition, hypervelocity regime, RANS, Hybrid LES/RANS, filtered mass density function, reduced chemical kinetics, ignition delay, RCCS, ISAT | | | | | |
| 16. SECURITY CLASSIFICATION OF: | | | 17. LIMITATION OF ABSTRACT | 18. NUMBER OF PAGES | 19a. NAME OF RESPONSIBLE PERSON |
| a. REPORT | b. ABSTRACT | c. THIS PAGE | | | James C. McDaniel, Jr. |
| U | U | U | UU | 48 | 19b. TELEPHONE NUMBER (Include area code) 434-924-6293 |

INSTRUCTIONS FOR COMPLETING SF 298

1. REPORT DATE. Full publication date, including day, month, if available. Must cite at least the year and be Year 2000 compliant, e.g. 30-06-1998; xx-06-1998; xx-xx-1998.

2. REPORT TYPE. State the type of report, such as final, technical, interim, memorandum, master's thesis, progress, quarterly, research, special, group study, etc.

3. DATES COVERED. Indicate the time during which the work was performed and the report was written, e.g., Jun 1997 - Jun 1998; 1-10 Jun 1996; May - Nov 1998; Nov 1998.

4. TITLE. Enter title and subtitle with volume number and part number, if applicable. On classified documents, enter the title classification in parentheses.

5a. CONTRACT NUMBER. Enter all contract numbers as they appear in the report, e.g. F33615-86-C-5169.

5b. GRANT NUMBER. Enter all grant numbers as they appear in the report, e.g. AFOSR-82-1234.

5c. PROGRAM ELEMENT NUMBER. Enter all program element numbers as they appear in the report, e.g. 61101A.

5d. PROJECT NUMBER. Enter all project numbers as they appear in the report, e.g. 1F665702D1257; ILIR.

5e. TASK NUMBER. Enter all task numbers as they appear in the report, e.g. 05; RF0330201; T4112.

5f. WORK UNIT NUMBER. Enter all work unit numbers as they appear in the report, e.g. 001; AFAPL30480105.

6. AUTHOR(S). Enter name(s) of person(s) responsible for writing the report, performing the research, or credited with the content of the report. The form of entry is the last name, first name, middle initial, and additional qualifiers separated by commas, e.g. Smith, Richard, J, Jr.

7. PERFORMING ORGANIZATION NAME(S) AND ADDRESS(ES). Self-explanatory.

8. PERFORMING ORGANIZATION REPORT NUMBER. Enter all unique alphanumeric report numbers assigned by the performing organization, e.g. BRL-1234; AFWL-TR-85-4017-Vol-21-PT-2.

9. SPONSORING/MONITORING AGENCY NAME(S) AND ADDRESS(ES). Enter the name and address of the organization(s) financially responsible for and monitoring the work.

10. SPONSOR/MONITOR'S ACRONYM(S). Enter, if available, e.g. BRL, ARDEC, NADC.

11. SPONSOR/MONITOR'S REPORT NUMBER(S). Enter report number as assigned by the sponsoring/monitoring agency, if available, e.g. BRL-TR-829; -215.

12. DISTRIBUTION/AVAILABILITY STATEMENT. Use agency-mandated availability statements to indicate the public availability or distribution limitations of the report. If additional limitations/ restrictions or special markings are indicated, follow agency authorization procedures, e.g. RD/FRD, PROPIN, ITAR, etc. Include copyright information.

13. SUPPLEMENTARY NOTES. Enter information not included elsewhere such as: prepared in cooperation with; translation of; report supersedes; old edition number, etc.

14. ABSTRACT. A brief (approximately 200 words) factual summary of the most significant information.

15. SUBJECT TERMS. Key words or phrases identifying major concepts in the report.

16. SECURITY CLASSIFICATION. Enter security classification in accordance with security classification regulations, e.g. U, C, S, etc. If this form contains classified information, stamp classification level on the top and bottom of this page.

17. LIMITATION OF ABSTRACT. This block must be completed to assign a distribution limitation to the abstract. Enter UU (Unclassified Unlimited) or SAR (Same as Report). An entry in this block is necessary if the abstract is to be limited.

CENTER FOR HYPERSONIC COMBINED CYCLE FLOW PHYSICS

I. Introduction

Airbreathing propulsion systems are attractive for hypersonic flight vehicles for applications such as high-speed, long-distance strike or access to orbit. In the latter case, the primary benefit relative to traditional rockets is that the airbreather does not have to carry its oxidizer on board, providing a potential payload fraction advantage. Relative to a rocket, however, the hypersonic airbreather will be a much more complex system, considering the external physics of high-speed aerothermodynamics and the complex propulsion flowpath physics. The airbreathing propulsion system will be a combined cycle, since no one currently-known cycle can operate from takeoff to high-speed cruise, or to rocket takeover for final boost to orbit. Two combined cycle systems currently under consideration are the rocket-based combined cycle (RBCC) and the turbine-based combined cycle (TBCC). In the current TBCC design concepts, the turbine flowpath is located parallel to and above the high-speed ramjet/scramjet flowpath and is closed off after ramjet takeover. The process of transitioning from the low-speed turbine flowpath to the high-speed flowpath is the first critical combined cycle mode transition. The acceleration through the ramjet mode to the scramjet mode represents the second critical transition, the dual-mode. The vehicle is operated in supersonic/hypervelocity modes for the high-speed strike mission, or up to scramjet-to-rocket takeover Mach number for a two-stage-to-orbit (TSTO) vehicle. The Center concentrated on the physics of the complex fluid mechanics and combustion phenomena, and their interaction, in the combined cycle airbreathing flowpath.

The design of optimal hypersonic air breathing combined cycle propulsion systems poses the following challenges to the nation's future capability for high-speed flight and access to space:

1. Accomplishing the low-speed turbine-to-ramjet transition while maintaining good inlet characteristics without unstart. The Center utilized the IMX and LIMX experiments at NASA Glenn to study this transition.
2. Accomplishing the ramjet-to-scramjet transition with good combustion efficiency while holding the shock train in the isolator in the dual-mode regime. The Center used the dual-mode combustion tunnel at UVA to investigate this mode transition.
3. Maintaining good combustion efficiency in the hypervelocity regime where mixing is diffusion-limited and dominates the combustor physics. The NASA HyPulse facility at ATK GASL was used to study this regime.

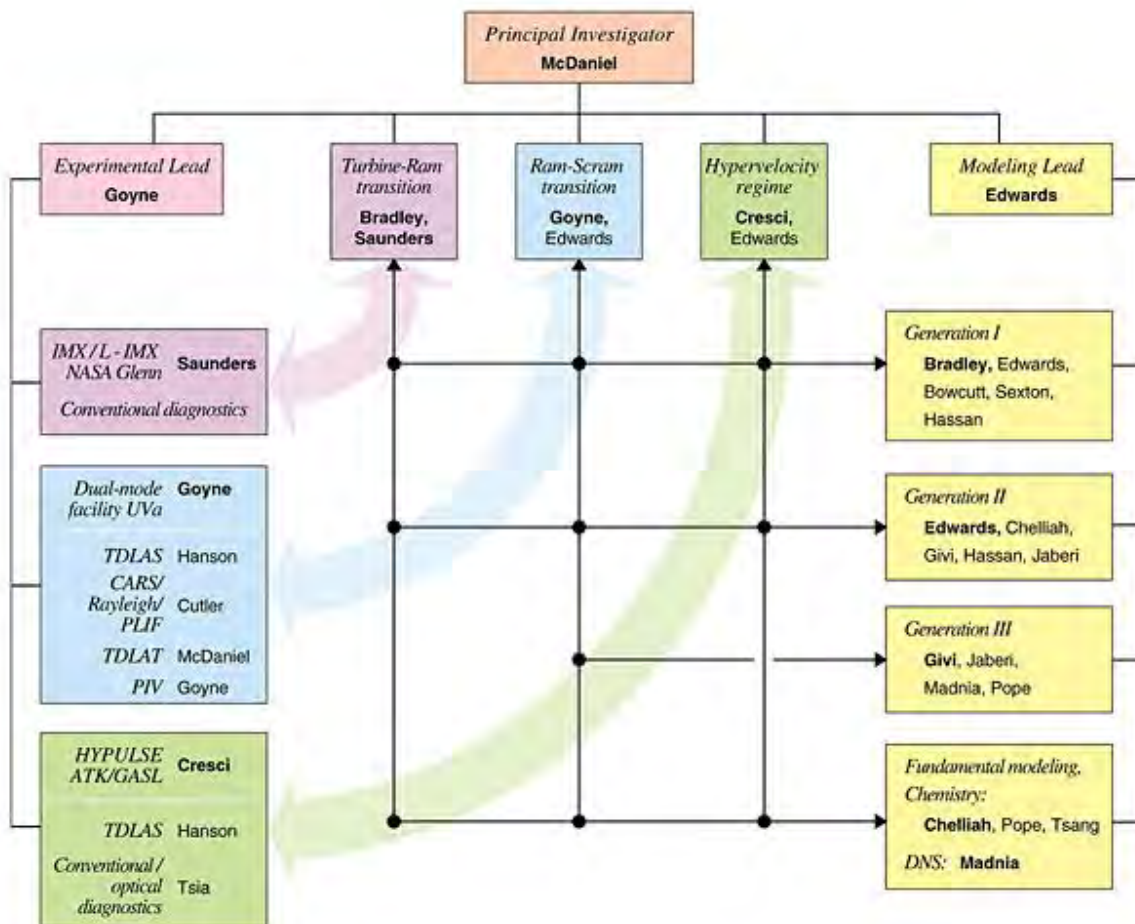
The objective of the Center for Hypersonic Combined Cycle Flow Physics was to advance the understanding of the critical mode transitions and supersonic/hypervelocity flow regimes of combined cycle propulsion by:

1. Developing an advanced suite of computational modeling and simulation tools for predicting combined cycle flow physics by collecting into one center some of the best modelers of high speed reacting flows,

2. Utilizing the unique facilities available to the Center and a group of the leading experts in advanced flowfield diagnostics to conduct experiments that will:
 - a. Provide insight into the fundamental physics of the complex flow in combined cycle hypersonic propulsion systems,
 - b. Provide detailed data sets for the development and validation of models of combined cycle flow physics, and,
3. Bringing together the modelers and experimentalists in a synergistic way to work on common problems in hypersonic combined cycle propulsion such that the resulting team provides an impact that far surpasses that available with individual investigator efforts.

II. Management structure

The management structure of the Center is shown below. This structure was maintained through years 1 to 3 of the Center.



When the NASA funding was withdrawn, the structure for years 4 and 5 was changed as below:

Jim McDaniel – PI

Chris Goyne – dual-mode facility lead

Andrew Cutler – CARS/PLIF lead

Jack Edwards – numerical modeling lead

Harsha Chelliah – chemistry modeling lead.

III. Research in years 1-3

The following describes the research conducted by the investigators in years 1-3 of the Center.

A. Experimental:

1. TBCC Dual-Inlet Mode Transition: Boeing (Marty Bradley and Kevin Bowcutt)

Experimental data was provided to Boeing from the NASA Glenn IMX and LIMX experiments. Boeing's objective was to simulate the complex flowpath in the dual-flowpath inlets with boundary layer bleed, by applying a RANS CFD code. Accurate prediction of the compression efficiency, flow distortion and operability was desired. It was found that modeling the entire complex inlet systems was not possible without focusing on the detailed physics of the shock/boundary/layer interaction with bleed. A full bleed model was developed, with bleed holes and bleed plenum (this work was conducted in conjunction with NCSU). It was found that a surface bleed pattern model, without plenum, was sufficient to match the surface pressure distribution measured in the LIMX experiment. RANS predictions showed the total pressure recovery and flow distortion to be highly time-dependent at the turbine inlet plane, in agreement with the experiment. If the research were continued, Boeing would investigate a statistical analysis of inlet recovery and flow distortion parameters using a time-dependent RANS solution.

2. Dual-Mode Transition: (Goyne and McDaniel)

a. UVa Configurations A and C

Configuration A

Figure 1 shows a cross-sectional view of the Configuration A flow path. This was the first and shortest flow path studied by the Center. It starts with a two-dimensional Mach 2 facility nozzle and has a short constant area section upstream of an unswept ramp fuel injector. Hydrogen fuel injection is through a Mach 1.7 conical nozzle in the base of the ramp that is parallel to the face of the ramp. Measured pressure distributions at two different fuel equivalence ratios are also shown in figure 1. This flow path was operated only in the scramjet mode of combustion with no shock

train upstream of the fuel injector. This experimental flow path geometry was chosen with significant consideration given to the requirements of CFD validation. In particular, the inflow to the combustor is as close to the exit of the facility nozzle as possible. Fuel equivalence ratios and heat release in the combustor are limited such that a thermal throat is not achieved making the combustion process supersonic in a one-dimensional sense. These conditions reduce the thickness of the boundary layer upstream of fuel injection and preclude a pre-combustion shock train, making it easier to quantify the inflow experimentally and simulate the flow numerically.

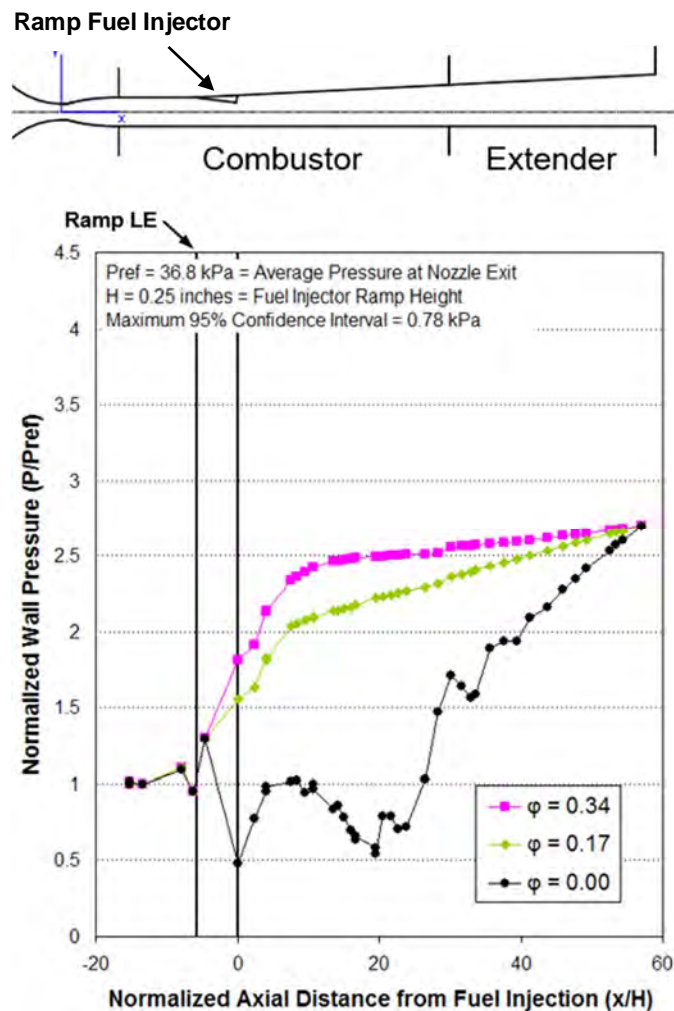


Figure 1. Configuration A flowpath and normalized wall pressures.

Configuration C:

Figure 2 shows a cross-sectional view of the Configuration C flow path. This flow path incorporates several elements from Configuration A, including the unswept ramp hydrogen fuel injector. A constant area isolator is included upstream of the combustor to contain any pre-combustion shock train and a constant area section downstream of the combustor helps stabilize combustion and induces the formation of a thermal throat in the dual mode. Measured pressure

distributions at several fuel equivalence ratios are shown, which illustrate the dual-mode nature of this flow path. The scram mode with no pre-combustion shock train is achieved at equivalence ratios below approximately 0.2. At equivalence ratios above 0.38, the flow at the ramp leading edge is subsonic in a one-dimensional sense and the flow path operates in a ram mode of combustion. At intermediate equivalence ratios, an oblique shock train is present in the isolator although the flow is still estimated to be supersonic at the ramp leading edge in a one-dimensional sense.

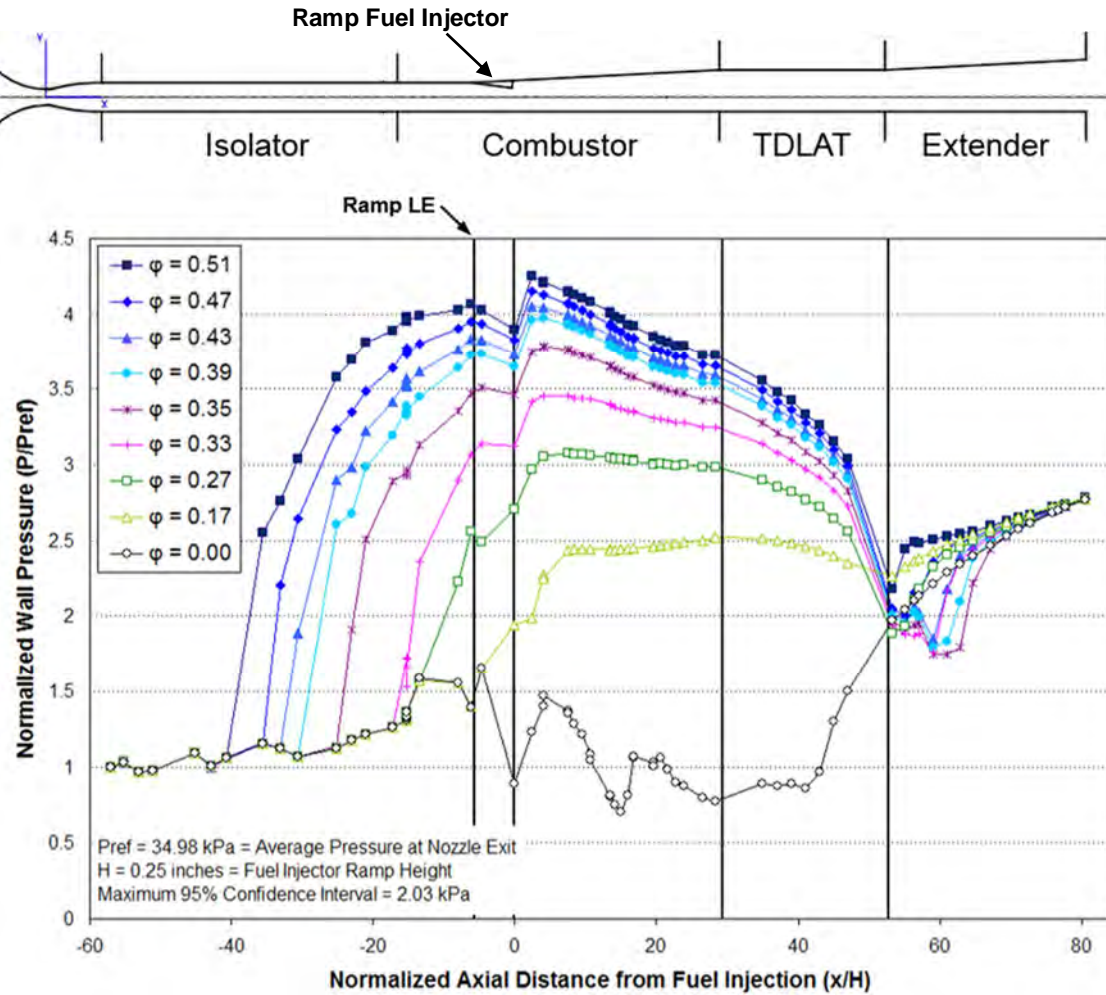


Figure 2. Configuration C flowpath and normalized wall pressures.

b. Flow diagnostics

1) SPIV: UVa (Goyne)

A stereoscopic particle image velocimetry (SPIV) system was applied to five measurement planes in Configuration C. This system acquired data at 10 Hz and was used in conjunction with 250 nm

silicon dioxide tracer particles. As an example of the data collected, Fig. 3 depicts mean velocity magnitude in the combustor crossplane at $x/H=12$. This result was generated from an ensemble average of 2000 instantaneous velocity fields at a spatial resolution of 3 vectors per millimeter. The plot on the left depicts scramjet-mode operation, where the velocity of the partially-separated flow downstream of the ramp fuel injector (bottom of plot) is substantially lower than that of the supersonic freestream (top of plot), and counter-rotating vortices induced by the ramp injector draw high-momentum freestream flow down along the side walls toward the injection wall. When equivalence ratio is increased from $\phi=0.18$ (left plot) to $\phi=0.49$ (right plot), transition to dual-mode operation occurs. The plot on the right in Fig. 3 shows SPIV measurements in this dual-mode regime. Heat release from combustion and the resulting shock train decrease freestream velocity to subsonic values, and the flow is now dominated by the higher momentum of the fuel jet

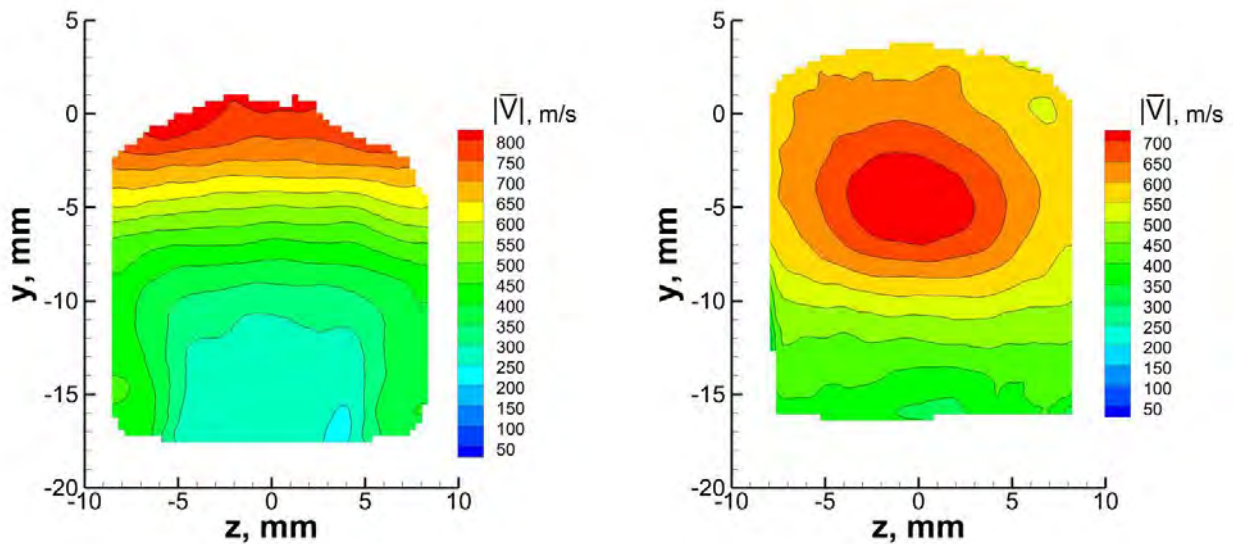


Figure 3: SPIV measurements: scramjet mode on left, dual-mode on right

2) CARS and OH PLIF: GWU (Cutler)

This work included development and validation of dual-pump coherent anti-Stokes Raman spectroscopy (CARS) and OH planar laser induced fluorescence instrumentation in laboratories at NASA Langley Research Center and transportation of the equipment to the University of Virginia's (UVA) Aerospace Research Laboratory for two lengthy test campaigns (returning the equipment to NASA Langley in between campaigns). Software for the analysis of CARS spectra data was developed. Extensive experimental databases of flow temperature (both rotational and vibration of nitrogen), and mole fraction concentrations of N_2 , O_2 , and H_2 were generated with the CARS instrument, and extensive planar imaging of the OH radical was performed using PLIF. Databases were acquired in both the "Configuration A" and "Configuration C" configurations of the UVA dual-mode scramjet. These configurations are hydrogen fueled from single ramp injectors. The databases have been shared with the computational fluid dynamics community for computational model development, including extensive modeling at the Center by Jack Edwards (NC State).

Some typical CARS and OH-PLIF results are presented in Fig. 4. Figure 4(a) is a scatter plot of CARS-measured temperature vs mixture fraction at several points in the reacting fuel-air plume (as indicated in the inset image) for the Configuration C scramjet mode ($\Phi=0.18$), plane 2 ($x/h=18$). This plot indicates near equilibrium in some portions of the flow and strong burning in others. Figure 4(b) is an OH-PLIF image at the same location and operating condition, showing the regions with OH present (the flame post-reaction region) and indicating a turbulent flame surrounding an unsteady fuel rich central core. These results have been published extensively.

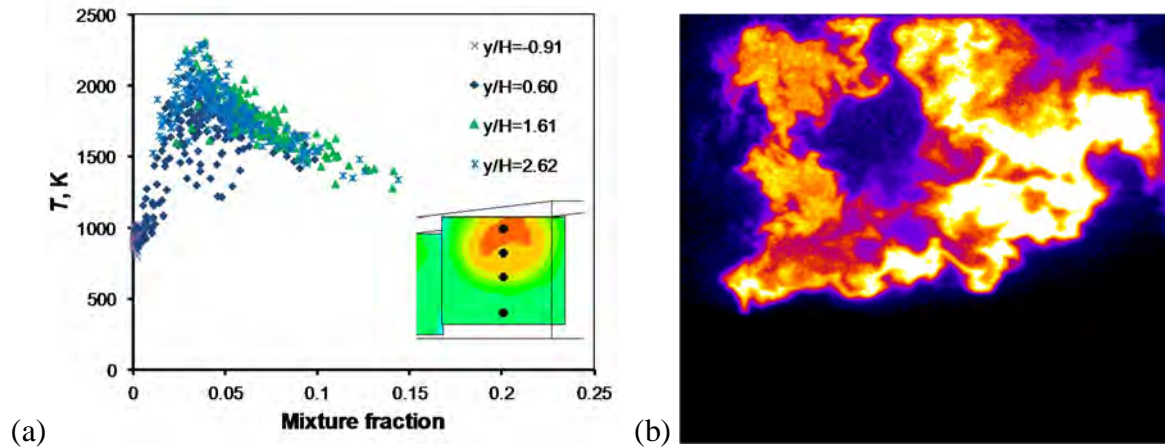


Figure 4. Typical CARS and OH-PLIF results for Configuration C scram case, plane 2

Some findings based on these measurements (excluding those findings enabled by comparison with modelling efforts reported by Edwards) include the following:

- High quality simultaneous, spatially and temporally resolved CARS measurements of temperature (including separate rotational and vibrational temperature of N_2), N_2 , O_2 and H_2 concentration, including statistics (such as means, variances, covariances, histograms, and scatter plots, etc.) were obtained in a scramjet combustor. This has never been done before.
- Details of flame holding in both scramjet (low-fuel-air equivalence ratio) and ramjet (high fuel-air equivalence ratio) cases were observed.
- Vibrational non-equilibrium in the free stream of the facility flow was discovered, with vibrational temperatures of N_2 being at the facility stagnation temperature. Working with Baurle at NASA Langley, we showed that this non-equilibrium could be predicted using existing models and data from the literature.
- OH-PLIF imaging yielded details of the instantaneous flame (spatial) structure

3) TDLAS: Stanford (Hanson)

A new laser diagnostic technique was developed and applied in the UVa dual-mode facility for time-resolved measurement of water vapor. The technique was developed as a form of TDLAS (tunable diode laser absorption spectroscopy) for flows where line-of-sight measurements are not

sufficient. By selecting an absorption transition for which the product of line strength and temperature are constant, a measurement is made of “column density.” This measurement is not limited by the assumption of constant density along the optical path, as with the standard TDLAS approach. This is the first time that this approach has been proposed and was applied to measurements in the UVa configurations A and C. Comparisons were made to CFD measurements. It was concluded that the column density approach agreed with CFD in the hydrogen fuel injection plume, with disagreement outside the plume. The reason for this disagreement was not determined.

4) TDLAT: UVa (McDaniel)

In flows which are highly three-dimensional, a method was developed for producing time-resolved planar measurement of water vapor concentration and temperature in a supersonic combustor. The technique was based on TDLAS, using multiple beam paths and a tomographic reconstruction. The technique is referred to as Tunable Diode Laser Absorption Tomography. Measurements were made at the exit of the UVa dual mode facility, in a nonreacting case with steam injection into the tunnel, and in the reacting flow. The TDLAT measurement was combined with SPIV measurement at the combustor exit plane to measure the combustion efficiency. Good comparison of the combustion efficiency measurement with CFD was found when the tunnel was operated in the scram mode. It was found that the combustion efficiency was higher when the tunnel was operated in the ram mode than the scram mode. This was counter to the view that the steamwise vortices generated by the ramp fuel injector, which enhance the mixing of the fuel with the incoming air, are weaker in the ram mode. No CFD was available in the ram mode to verify this finding.

4. Hypervelocity Regime: GASL (Goynes and Cresci)

The NCHCCP Hypervelocity group conducted Mach 7 testing in the HYPULSE facility, generated a quantitative data set for CFD model development and validation, and gathered experience in implementing a Tunable Diode Laser Absorption Spectroscopy (TDLAS) system in a pulsed, hypervelocity facility. These activities contributed to reaching the objectives of (1) measurement of reacting flow turbulence statistics and novel fuel-air mixing and flame holding schemes through the development and application of advanced diagnostics, and (2) development of benchmark data sets with quantified experimental uncertainty for the purposes of developing accurate RANS, hybrid LES/RANS, and LES models.

The group’s approach was to utilize an existing high speed engine (shown in Figure 5), donated to the program by the High Speed System Test (HSST) group, a focus area sponsored by the Office of the Secretary of Defense’s Test Resource Management Center, install it into the HYPULSE facility and conduct a series of tests at hypervelocity conditions. In HYPULSE, the test times are on the order of milliseconds, but a wide array of measurements and non-intrusive diagnostics can be employed to meet various program objectives. For this program, standard high speed pressure and heat flux measurements were made throughout the engine, high speed Schlieren photography utilized newly fabricated engine optical access ports, and, finally, an advanced TDLAS multipath

technique was utilized to gather quantitative measurements at the same critical flow path locations as gathered in the dual-mode engine tests that were conducted at the University of Virginia.

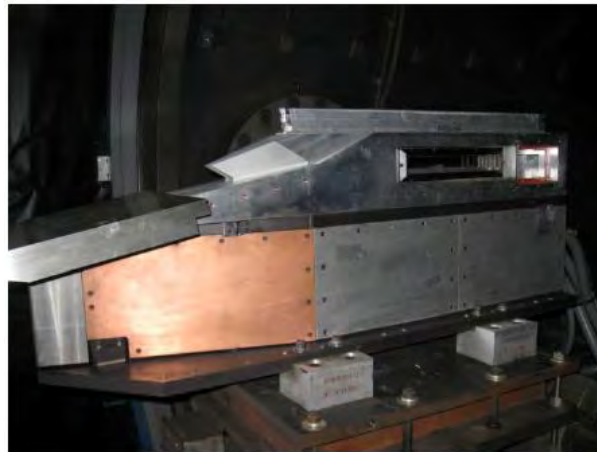


Figure 5. Hypervelocity test article installed in HYPULSE facility

Figure 6 shows engine flowpath pressure profiles for a typical test, in which engine pressures are low during fuel off conditions, i.e. tare, but then increase significantly when fuel is added to the combustor region, indicating stable combustion and flame holding capabilities. 20% silane in hydrogen was used as fuel.

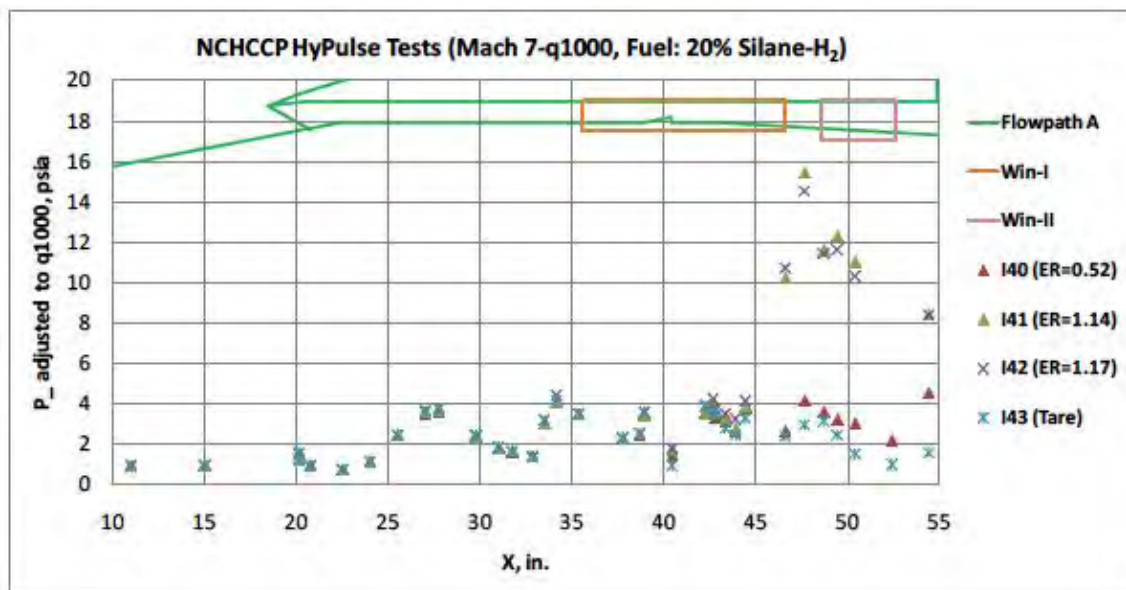


Figure 6. Pressure profiles indicating stable combustion and flameholding

The TDLAS system performed well, showing generally consistent results with the pressure and heat flux measurements, across 3 of the 5 Lines of Sight (LOS) achieved by the first generation

laser beam pitch/catch optical mounts. The 2nd generation multi-LOS system was also applied that utilized larger collection optics and separated the degrees-of-freedom for alignment of each LOS. TDLAS data interpretation proved difficult due to the noisy pressure measurements and the required filtering. Work was also conducted to reinterpret the absorption in terms of column density which reduced the data analysis sensitivity to these pressure measurements.

The numerical modeling results showed general agreement with experimental test results, but were unable to match experimental results with a standard or modified combustion model, as shown in Figure 7. One of the issues is that existing silane combustion models are not valid at low temperatures or usable on large grids. Indications are that the solidification of SiO₂ should probably be modeled using finite-rate chemistry as well. Further work is required to address these issues.

Lessons learned during the program included:

- The flowpath was not well suited for the hypervelocity regime as stable flameholding could only be achieved with a mixture of silane and hydrogen as the fuel,
- The TDLAS measurements indicated driver gas contamination occurred earlier in the test window than previously measured,
- The shock heated environment of an impulse facility is a difficult and challenging application of flow diagnostics due to the transient nature of the flow and facility operation,
- Performing fundamental research using a large commercial experimental facility is fiscally challenging.

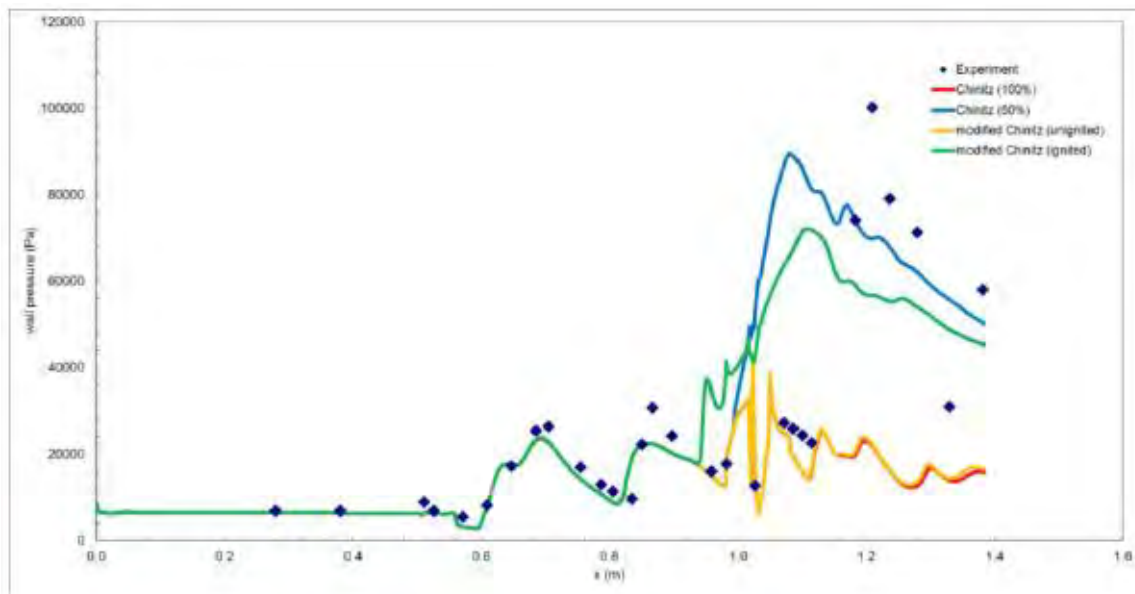


Figure 7. Modeling results showing inconsistencies with experimental results

B. Numerical modeling: (Edwards)

Numerical modeling efforts within the Center were divided into three Generations. Generation I represents state-of-the-practice Reynolds-averaged Navier-Stokes (RANS) modeling. Generation II represents hybrid large-eddy simulation / Reynolds-averaged Navier-Stokes (LES/RANS) modeling as well as scalar filtered-density function (S-FDF) LES modeling of high-speed reactive flows. Generation II models can be viewed as the current state of the art. Generation III models are represented by the energy-pressure-frequency-velocity-scalar FDF (EPFVS-FDF), which represents the most advanced version of the particle-based FDF LES methodology.

Generation I (RANS models; NCSU (Edwards, Hassan), Boeing (Bowcutt, Sexton, Bradley))

Generation I models were used to simulate NASA Glenn's dual flow-path TBCC inlets and ATK-GASL's Hypulse sub-scale engine rigs. For the former application, Boeing and NCSU conducted simulations of NASA Glenn's IMX and LIMX dual flow-path TBCC inlets. The challenge in these simulations is in maintaining the terminating shock at a stable position in the low-speed (turbine) inlet flow path. Experimental data from the IMX experiment was used by both groups; only Boeing had access to the experimental data for the larger L(arge)IMX configuration, as it was registered as ITAR. The IMX data consists of wall pressure measurements and global bleed flow rates for all of the bleed areas. The experimentalists were not able to close the mass balance, implying that some leakage occurred. Boeing simulations utilized a fixed-bleed boundary condition that imposed a constant bleed flow rate for each bleed region. NCSU simulations used an immersed-boundary (IB) method to simulate the effects of individual bleed holes. In the IB method, strategies are used to detect the embedded bleed plates, and boundary conditions are applied to force (indirectly) a no-slip condition. Plenum chambers were also modeled in the NCSU simulations. To ensure a high level of isotropic mesh resolution in the vicinity of the bleed holes, the NCSU simulations used various patched-mesh strategies, leading to an overall cell-count in excess of 12 M for a mesh with half-plane symmetry. Even with enhanced fidelity in modeling the bleed process, the NCSU simulations were generally unsuccessful, as the terminating shock eventually moved upstream and unstabilized the inlet. The shock was more stable in the Boeing simulations, and they were able to obtain adequate agreement with experimental data after careful adjustment of the bleed parameters.

Experiments involving hydrogen combustion at Mach 5, Mach 7, and Mach 10 enthalpy were conducted at ATK-GASL's HYPLUSE facility using a scramjet inlet / isolator / combustor model that was similar to that tested at UVA in direct-connect mode. Companion CFD simulations were conducted by NCSU using RANS turbulence models with finite-rate chemistry. The experimental rig was unable to sustain combustion at Mach 5 and 7 enthalpies without using the pyrolytic agent silane. As there was no established, affordable reaction model for combustion of silane / hydrogen mixtures at conditions relevant to the HYPLUSE experiments, a significant effort was undertaken by NCSU and UVA to identify potential reduced mechanisms suitable for incorporation into a detailed calculation. One mechanism containing 25 species was found to perform adequately at Mach 7 but did not completely predict the combustor pressure levels observed in the experiment. Weak ignition using only hydrogen was predicted by a 9-species hydrogen oxidation model at Mach 10 enthalpy conditions, but the level of heat release was very small.

Generation II (LES/RANS and S-FDF models; NCSU (Edwards), MSU (Jaberi))

LES/RANS

LES/RANS models suitable for high-speed reactive flows in complex geometries were developed by NCSU as part of the Center. Elements of the methodology include hybrid piecewise parabolic method / central-difference discretization schemes, synthetic turbulence inflow generation procedures, provision to incorporate systematically-reduced reaction mechanisms, and provision to incorporate non-uniform inflow conditions determined from experimental data. The models used a LES/RANS hybridization strategy developed under a grant from the Army Research Office. Various simple closure models for the effects of subgrid turbulent fluctuations on chemical production rates were also tested. These include algebraic and transport-equation based PaSR models, scale-similarity models, and hybrid PaSR / scale-similarity models. Typical calculations used from 33 to 93 million mesh cells, and meshes were generated using either Gridpro or Gridgen.

LES/RANS reactive calculations were performed for three UVa rigs (Configurations A, C, and E) during the first four years of the Center. The Configuration A rig was designed for scram-mode supersonic combustion of hydrogen, injected behind a wedge-shaped flameholder. The rig did not contain an isolator, and the mesh generated for these calculations contained about 33 M cells. Initial calculations were performed in an essentially ‘blind’ manner, as only wall pressure data was available before the calculations were started. Nevertheless, generally excellent agreement with available CARS, SPIV, focused Schlieren, OH-PLIF, and TDLAS data was obtained using the Jachimowski hydrogen oxidation model. Subsequent simulations were performed to identify sensitivities to factors such as inflow non-uniformity, choice of reaction mechanism, various subgrid closure models, and numerical discretization. These sensitivities were quantified using relative and absolute error analysis, revealing that the choice of reaction mechanism was by far the most sensitive factor.

The next set of calculations was performed for the Configuration C rig, which included an isolator and a straight section in the combustor that was used to facilitate TDLAT measurements. Calculations were performed in both scram and ram mode, with the former situation extensively analyzed using various subgrid closures and inflow generation techniques. A mesh containing 70 M cells was used for these calculations. Calculations performed under ram-mode conditions tracked the upstream progress of the isolator shock train. In both cases, results were compared with CARS, SPIV, wall pressure, OH-PLIF, TDLAS, and TDLAT measurements. Only the Burke, et al. (2011) hydrogen oxidation mechanism was employed in these calculations. One conclusion of these studies was that the inflow generation method used in some calculations (a recycling / rescaling strategy), led to excessively energetic turbulent structures in the isolator and to an over-mixing of reactants. Enforcing a RANS inflow (accurate only for scram-mode calculations) alleviated the over-mixing effect and enabled excellent agreement with available experimental data. Sensitivities to other factors were not as pronounced, though some PaSR subgrid-closure variants did result in flame detachment from the wedge, in contrast with experimental observations. The Configuration C scram-mode LES/RANS database was used to investigate the utility of strained laminar flamelet theory as a means of analyzing combustion characteristics. The analysis showed that vortices shed from the flameholder, while effective in enhancing mixing,

lead to very high local strain rates in parts of the flame, causing regions of local extinction. Flame stabilization occurs within low-momentum regions at the base of the flameholder, where strain rates are lower and residence times are higher.

Scalar Filtered Density Function Methods

A significant effort was undertaken to further the development of FDF (filtered density function) turbulence closure methods as part of the Center. FDF methods are Lagrangian particle-based methods in which a notional particle contains the composition (and sometimes) velocity, subgrid scale turbulence, pressure, and energy of the system. Stochastic partial differential equations are evolved to vary these quantities, with the randomness inherent in such equations representing the general ‘randomness’ induced by unresolved subgrid-scale fluctuations. The main advantage of FDF methods is that subgrid-scale effects of turbulence on reaction source terms are represented in closed form. The main disadvantage is that a large number of notional particles are required in mesh cells that are thermodynamically active, necessitating complex methods for integrating large numbers of particles, statistically sampling (or filtering) the results over each mesh cell, and coupling the filtered data obtained from the particle method (if necessary) with an Eulerian flow solver.

Researchers at Michigan State University developed ways of extending the scalar FDF (S-FDF) model to handle flows with shock waves. The S-FDF methodology couples scalar and temperature fields obtained from the particle methods with velocity, pressure, and subgrid-scale turbulence fields obtained from conventional Eulerian LES models. They utilized a modified version of the MP-DATA higher-order reconstruction method of H.T. Huyhn to resolve fine-scale turbulent features as well as shock waves. They also developed improved ways of coupling the particle methods with the Eulerian solvers so that the correct pressure jump through shock waves could be obtained. They used simulations of rapid compression machines and reactive and non-reactive hydrogen-air shear layers to assess their models. Later efforts by this group focused on notional cavity flameholders and on the generation of DNS data suitable for use in improving the more advanced FDF models discussed later. The MSU researchers did not attempt to simulate the UVA experiments with their models, as their research code was unable to handle the size and the geometric complexity of the combustors.

Generation III (EPVFS-FDF models; U. Pittsburgh (Givi), U. Buffalo (Madnia))

Researchers at the University of Pittsburgh focused on the development of perhaps the most advanced FDF model, the energy-pressure-frequency-velocity-scalar (EPFVS) FDF. Major challenges in closing various terms in the stochastic equations for energy and pressure were revealed. DNS simulations of canonical compressible turbulent flows were conducted by the University of Buffalo in an attempt to provide data suitable for model development. No tests of the model for conditions relevant to high-speed combustion were performed by the end of the fourth year of the Center. The University of Pittsburgh made major advances in the design of parallel algorithms for solving FDF stochastic transport equations. They developed a domain decomposition method for the ensemble of FDF notional particles termed the ‘irregular portioning method’. This approach allowed scalability of their particle-transport solver (using the S-FDF

model) to thousands of CPU cores. They applied their approach to premixed Bunsen-burner flames as well as to the Sandia ‘D’ flame.

Summary and Overall Appraisal

In all, several models for simulating high-speed, turbulent reactive flows were developed as part of the Center. As discussed in the detailed description above, not all models were advanced to the point that they could be applied to the UVa experiments or to other relevant experiments. A brief summary of the state of the development of each class of model is as follows:

Generation I (RANS)

- No major advances in RANS turbulence modeling were attempted.
- Protocols to embed stereolithography (STL) renderings of embedded immersed objects into a compressible CFD simulation were developed as part of NCSU’s work on the TBCC dual flow path
- New reduced reaction mechanisms for silane / hydrogen combustion were developed and tested with respect to the high-enthalpy experiments performed at the Hypulse facility.

Generation II (LES/RANS and S-FDF)

- Techniques developed to use experimental CARS data to model inflow non-uniformity as part of a general focus on ensuring fidelity to a particular experiment with as few assumptions as possible.
- Several simple closures for accounting for the effects of un-resolved turbulent fluctuations on species production rates were developed and tested versus UVa data as part of the NCSU activity. Models considered included PaSR variants, quadrature-based models, and scale-similarity models. No consensus emerged as to the superiority of one such model relative to the others.
- Strategies for embedding source terms from systematic reaction-reduction techniques into the NCSU LES/RANS framework were developed and successfully tested for ethylene combustion.
- Strategies for effectively coupling S-FDF particle fields with Eulerian continuum fields for strongly compressible flows were developed and tested, as were high-resolution numerical schemes for compressible turbulence.
- Several DNS studies of hydrogen-air combustion were performed and the data used to assess aspects of the S-FDF closures.

Generation III (EPFVS-FDF)

- The formulation of the system of stochastic PDEs that constitute the EPFVS-FDF closure was completed and attention directed to modeling unclosed terms with guidance from DNS data obtained for canonical compressible flows.
- Highly parallel domain-decomposition methods for integrating the particle equations were developed and tested for low-speed premixed and non-premixed flames.

Only the RANS and LES/RANS models developed by NCSU were used to simulate Center experiments, even though the other groups were strongly encouraged to do so. Efforts were made to exchange information between the modeling groups so that eventual one-to-one comparisons could be made. Examples include transitioning of non-uniform inlet conditions developed at NCSU to various groups (Center and others, such as M. Ihme's group at Stanford and Ez Hassan's activity at AFRL), as well as transitioning of logic for various subgrid closures among groups. The reality is that, within the Center, only the NCSU framework could handle the size and complexity of the UVa experiments without a significant effort in CFD algorithm development. Other issues, such as the presence of walls, thick boundary layers (under dual-mode conditions), reactions near walls, and non-uniform inflow boundary conditions, complicate the application of the particle-based methods to the UVa experiments (and to any realistic scramjet experiment). It appears clear that without a significant effort directed to extend S-FDF methods toward more complicated geometries and larger mesh sizes, there will be no way to truly assess this class of model's true potential for scramjet applications. Such efforts are underway, as innovations in parallel processing of particle-tracking solvers are made and as other groups become interested in the FDF methodology. In this author's opinion, however, one must be a 'true believer' of the FDF model's potential to invest resources, as the challenges associated with the paradigm shift encountered in moving from Eulerian to hybrid Eulerian / Lagrangian, to pure Lagrangian are immense. The benefits gained must greatly outweigh the costs in CPU and man hours expended. It will not be easy to perform a cost-benefit analysis for FDF or for any other class of advanced closure model because of institutional bias and because of the absence of a common platform that could effectively incorporate such models without a long development period.

The results obtained using the NCSU models (sometimes even under essentially 'blind' conditions) consistently illustrate the strong promise that LES holds for high-speed turbulent combustion, provided that the mesh is fine enough to resolve a flame thickness in ~two cells or less. While it is recognized that details of the internal structure of the flame cannot be obtained with this level of resolution, the effect at measurable scales (those consistent with experimental resolution) is qualitatively and (in many cases) quantitatively correct within experimental error estimates (repeatability being possibly the largest source of uncertainty for the UVa experiments). This does not mean that further improvements cannot be made – in particular, the NCSU LES/RANS models, when using 'laminar chemistry', consistently indicate a degree of over-prediction of temperature and major species production that is associated with the implicit assumption of a well-mixed environment within the subgrid. The deviations from experiment are not large, however, indicating that a well-designed SGS model may not have to be incredibly complex to bridge the gap. Some directions toward this design were undertaken as part of the Center and are being continued as part of current research.

C. Chemistry modeling: (Chelliah and Pope)

Turbulent reacting flow simulation of hypersonic flow fields using detailed chemical kinetic models with a large number of species and reactions is computationally prohibitive. Methods of simplifying or reducing chemical kinetic models for such complex reacting flow simulations was

the focus of this work. The effort was divided into two broad categories, (i) understanding the uncertainties associated with the current chemical kinetic and transport models, including supporting model validation experimental data, and (ii) development of model reduction strategies. It was deemed critical to understand the level of uncertainty of the chemical kinetic models to determine when to stop the model reduction process as reduced-order models inherently introduce uncertainties to the simulations.

1. Model and flame extinction uncertainty analysis:

While considerable literature exists on the uncertainties associated with reactant mixture ignition and flame propagation characteristics, the fundamental flame extinction data and their uncertainties were not well established. Thus, extensive effort was devoted to gather flame extinction limits and their uncertainties of cracked fuel species relevant for hypersonic propulsion systems, namely hydrogen, methane, ethylene, etc. (Sarnacki et al 2011). With regard to modeling, both chemical kinetic and transport parameter uncertainties controlling flame extinction limits were explored using extensive Monte-Carlo simulations with reported uncertainty bounds (Esposito et al. (2011) and (2012)). From these comprehensive analysis, it was shown that molecular transport coefficient uncertainties are same order as the counterflow extinction limit measurement uncertainties, while the chemical kinetic model parameter uncertainties were much greater than the experiments.

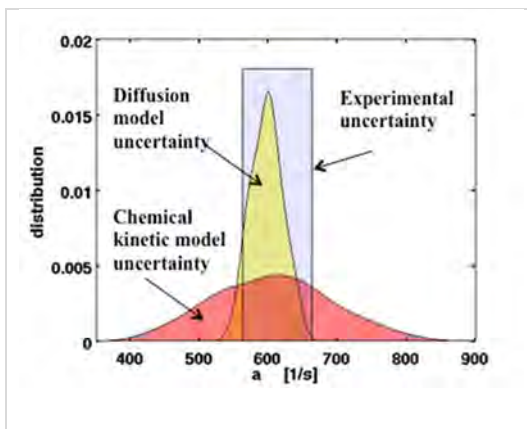


Figure 8: PDF of extinction strain rate uncertainty based on chemical kinetic model and diffusion coefficients, and counterflow experiments.

The main conclusion from these investigations was that counterflow flame extinction limit measurements can be used to reduce the chemical kinetic model parameter uncertainties but not the transport coefficients (see Figure 8). In addition, it was shown that fundamental canonical experiments could be performed at different pressure conditions in order to reduce the uncertainty of a specific reaction constant (Esposito et al (2012)), which is important at hypersonic engine operating conditions.

2. Model reduction strategies:

Principal Component Analysis using Sensitivities:

The majority of chemical kinetic model reduction strategies implemented in the literature are based on analysis of single phenomenon at a time, i.e. zero-dimensional ignition, one-dimensional

laminar flame propagation, or laminar flame extinction. Since all of the above phenomena can occur in the same elemental volume of a high-speed turbulent reacting flow, model reduction strategy based on the combined sensitivities of all the relevant phenomena was developed using the principal component analysis based on evaluated sensitivities (Esposito and Chelliah). In addition, a partially-stirred reactor (PaSR) frame work was implemented to test the PCAS based model reduction methodology in the presence of turbulent mixing (Rahimi et al., 2013). In the PaSR model, the flow of two or more streams of reactants are represented by reacting parcels or particles, which are allowed to mix and react inside the reactor under specific conditions. In particular, for certain characteristic mixing/residence time scales, the PaSR model may behave like a perfectly-stirred reactor (PSR) or a plug-flow reactor. In our PaSR analysis, the pair-wise mixing model described by Pope (1997) with specified mixing and pairing time scales was implemented. Figure 9 shows that as the number of species is reduced, the PCAS approach maintains a lower error compared to pure ignition only analysis indicating the importance of macro-scale mixing occurring in these turbulent reacting flows.

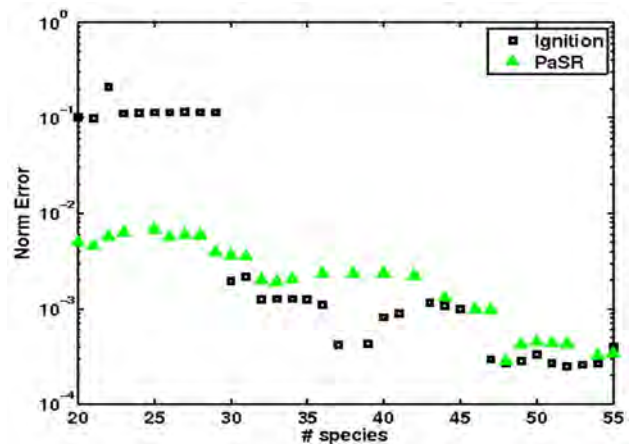


Figure 9: Error associated with model reduction using PCA, with sensitivity analysis of homogeneous ignition vs. PaSR.

In summary, the above results show that, as the number of species is reduced in PaSR simulations, PCAS of PaSR sensitivities yield much smaller error metric down to about 20 species while the PCAS of ignition delay sensitivities indicate a distinct jump in PaSR error at 30 species in the model.

In-situ adaptive tabulation (ISAT) and Rate-Controlled Constrained Equilibrium (RCCE)

In addition to skeletal reactions models extracted via the PCAS approach, it was shown that further computational savings could be achieved by using either quasi steady-state approximation (QSSA) or rate-controlled constrained equilibrium (RCCE) combined with In-situ adaptive tabulation (ISAT) in PaSR simulations (Hiremath and Pope, 2011).

In the past, the lack of an efficient method of identifying the constraint species in RCCE has hindered the application of this methodology. However, a new efficient algorithm was developed for identification of unrepresented species in PaSR simulations as the number of represented species were reduced from the skeletal model (Hiremath and Pope, 2013), identified by the acronym greedy algorithm with local improvement (GALI). A comparison of the error of PaSR simulations with the computationally efficient in-situ adaptive tabulation (ISAT) as a function of the number of represented (or transported) species in the RCCE simulations is shown in Figure 10, for two sets of conditions. The results clearly show that retaining the information of species associated with fast reactions via RCCE minimizes the reduction-tabulation error to about 5% with 20 represented species in the model.

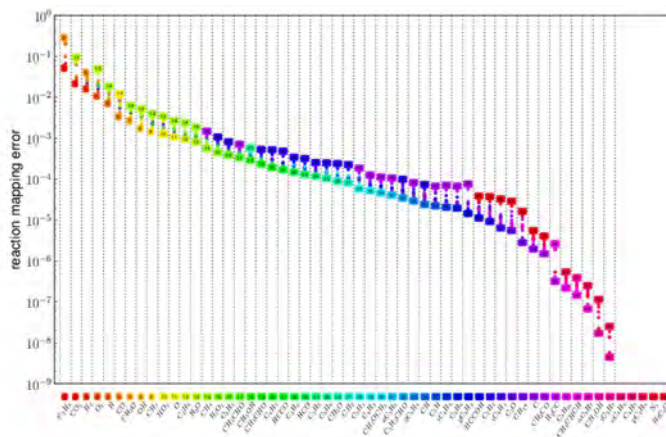


Figure 10: Error associated with model reduction using RCCE.

IV. Research in Years 4 and 5 (premixed flows)

In years 4 and 5 the research objective was to study compressible, turbulent, reacting premixed flows. The contribution of the investigators and key findings are summarized below.

A. Premixed High-speed Combustion in the UVa Dual-Mode Tunnel (Goyne and McDaniel)

1) Introduction

In order to gain a better understanding of the compressible, turbulent and reacting flow phenomena present in scramjet engines, a series of premixed fuel-air supersonic combustion experiments were conducted. The experiments involved combustion of ethylene fuel in air and the flame was anchored on a cavity. Both partially and fully premixed experiments were conducted. The examination of premixed combustion allowed the fuel-air mixing process to be decoupled from the combustion reaction process. The experiments reported here represent the first time a dual-mode scramjet has been operated under premixed conditions.

Research during the first three years of the Center focused on combustion in non-premixed flow and that work was performed largely with hydrogen as the fuel. Additional effort was devoted in year four to preparing for the fully premixed experiments to be conducted in year five of the Center. This was done in parallel with the planned experiments in year four by personnel who were partially supported by the Center and partially supported by a separate grant from AFOSR entitled, "Premixed Supersonic Combustion." According to the Statement of Work as defined in the original Center proposal, year five was to be devoted to shock wave control and innovative fuel injection schemes. While these investigations are important, it was felt that the premixed experiments were better aligned with the goals of the AFOSR. Since the premixed experiments were outside the original scope of the Center, funds from the "Premixed Supersonic Combustion" grant supported the additional costs to prepare for and conduct the premixed combustion experiments. Because of the complementary nature of the "Premixed Supersonic Combustion" and Center grants, the results from both grants are presented here.

The information presented below details the fuel-air premix approach and presents sample results. The information includes facility hardware, sample pressure scans, flowpath operability, combustion chemiluminescence, and mode transition.

2) Tunnel Hardware (isolator, injectors, cavity, throttle, etc.)

Experiments focused on ethylene fueling in what is termed the modified Configuration E flowpath as shown in Fig. 11. This flowpath starts with a 15.97 inch isolator that has a 1 inch by 1.5 inch rectangular cross-section. A 2.9° divergence on the cavity-side wall starts 2.1 inches upstream of the cavity leading edge. This divergence is maintained through the combustor and extender sections of the flowpath. A constant-area section compresses the flow downstream of the combustor inducing a thermal throat when the flowpath is operating in the dual-mode. The cavity flameholder spans the width of the duct and has an initial depth of 0.356 inches, which is maintained over a length of 1.22 inches. The cavity closes with a 22.5° ramp that terminates 2.1 inches downstream of the cavity leading edge. The flowpath exhausts into the laboratory at atmospheric pressure, 19.61 inches downstream of the cavity leading edge (40.8 inches from the exit of the Mach 2 facility nozzle).

The primary measurement locations are indicated in Fig. 11. The vertical green lines represent CARS measurement locations. Normalized by the cavity depth ($h = 0.356$ in.), these measurement planes are at axial locations of $x/h = -9.14, 2.39, 6.60,$ and 10.80 relative to the cavity leading edge. PLIF (OH and CH_2O) has been performed from the cavity leading edge to the downstream end of the optical windows in the duct, as indicated by the red box. The cavity-side wall is instrumented from inlet to exit with 80 low frequency pressure taps and 13 type K thermocouples that are primarily located on the combustor centerline.

All components are constructed of stainless steel with the exception of the cavity-side wall of the combustor, which is OFHC copper, and the large optical windows in the combustor, which are 0.375 inch thick fused-silica. Water cooling is incorporated in each component of the test-section and all stainless steel walls in the isolator, combustor, and constant area section are coated with a 0.015 inch thick layer of thermal barrier zirconia. The copper cavity wall is not coated.

Primary fuel injection is through two banks of six sonic, flush-wall injectors located in the isolator, 1.5 inches downstream of the facility nozzle on opposite walls of the duct. Each bank comprises two rows of three equally spaced 0.049 inch diameter injectors oriented normal to the freestream flow. NO PLIF measurements have verified that injection at this location allows the fuel to be processed in the isolator resulting in a fully premixed flow at the cavity leading edge.

Also shown in Fig. 11, a secondary fuel injection location is through a row of five equally spaced 0.021 inch diameter sonic, flush-wall injectors located 0.97 inches upstream of the cavity leading edge. The secondary injectors are too close to the cavity for the fuel injected through them to fully mix with the freestream and instead provide a means for more directly fueling the cavity. This allows the flowpath to operate in the scram mode with either a short or nonexistent precombustion shock train.

An air throttle is available downstream of the combustor, near the upstream end of the extender (at $x/h = 37.52$), which allows the duct to be back pressured independently or in conjunction with a combustion process. The air throttle is also used to facilitate ignition. The throttle consists of two slotted, high pressure air injectors, one in each side wall, that are used to restrict flow at that location. The slots are 0.125 inches wide and extend over the full height of the duct. Through use of the air throttle, it is possible to accurately locate and stabilize the leading edge of the isolator shock train at any point in the duct.

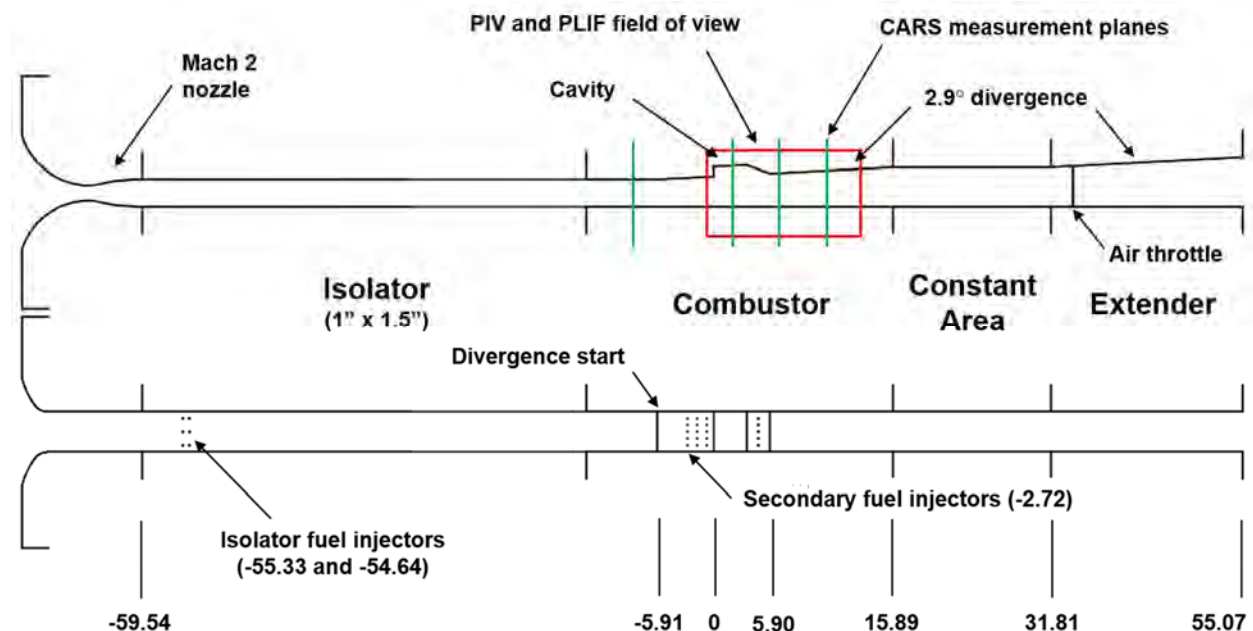


Figure 11. Modified Configuration E flowpath showing CARS measurement planes (green) and OH PLIF field of view (red): a) side view and b) top view with normalized axial distances from cavity leading edge (x/h).

3) Pressure Scans

Table 1 lists the test conditions for the main air flow. The given uncertainties are calculated by standard propagation of error and include temporal variability as well as instrumentation uncertainty. These flow conditions were typically maintained to less than $\pm 1\%$ during a run and across multiple runs. Table 2 lists the primary fueling conditions used in the experiments. The first fuel condition represents the maximum fuel rate that can be accommodated by the flowpath without unstating the isolator. The second condition is close to the lean flameout point of the flowpath with a fully premixed combustor inflow. The difference in the fuel injection pressures between the cavity-side bank and the opposite-side bank is due to a small difference in the discharge coefficients of the two injector banks (0.60 for the cavity-side bank and 0.56 for the opposite-side bank). The fueling may be evenly split between the two injector banks as shown in Table 2 or adjusted such that a larger proportion of fuel is delivered through the cavity-side bank.

Figures 12 and 13 show the axial distribution of static pressure on the cavity-side wall for global fuel equivalence ratios, ϕ , of approximately 0.40 and 0.34, respectively. The measured pressures have been normalized by the static pressure at the exit of the facility nozzle, P_{ref} , and the axial locations are normalized by the cavity depth (0.356 in.). Results for the case with all fuel being delivered through the cavity-side bank of injectors are shown along with two different fuel split ratios. The solid square symbols represent an equal fuel split and a uniform fuel-air premix. Also shown in the figures are the pressure distributions for the NO PLIF measurements, represented by a dashed line. In these cases the air throttle, rather than a combustion process, was used to generate the back pressure that drives the shock train in the isolator. It can be seen that the pressure rise in the isolator is the same whether it is due to a combustion process or the air throttle. The fuel off case is also shown for reference.

For both global fuel equivalence ratios, delivering all of the fuel through the cavity-side injectors alone will result in some level of fuel stratification across the duct with a higher density of fuel on the cavity-side wall. All fuel conditions shown in Figs. 12 and 13 result in a stable dual-mode scramjet flame anchored on the cavity that can be sustained for several hours in the facility. Using a one-dimensional model of the separated flow in the isolator, the Mach number at the cavity leading edge is estimated to be 0.70 for the $\phi = 0.40$ case and 0.72 for the $\phi = 0.34$ case.

While the pressures in the isolator and onset of the precombustion shock train are nearly the same for all three fuel splits, pressures are noticeably different in the combustor section between the cavity and the thermal throat (from $x/h = 5$ to 35). Here, the flow is subsonic in a one-dimensional sense and heat released in the flame drives the pressure down. It is evident that delivering all the fuel through the cavity-side injector bank results in an initially steeper drop in pressure in the vicinity of the cavity closeout ramp ($x/h = 5$) and lower combustor pressures overall when compared to the more uniformly premixed cases. In all combusting cases a thermal throat is formed at the downstream end of the constant area section ($x/h = 35$) indicating a transition back to supersonic flow. Thus, the combustion process is isolated from the atmospheric back pressure in these tests.

Table 1. Test conditions for main air flow.

| Parameter | Air | Uncertainty |
|-----------------------|------|-------------|
| Total pressure (kPa) | 300 | $\pm 1\%$ |
| Total temperature (K) | 1200 | $\pm 0.8\%$ |
| Mach number* | 2.03 | $\pm 1\%$ |

* Property at nozzle exit determined using nozzle area ratio and assuming isentropic flow ($\gamma=1.36$ for air).

Table 2. Test conditions for ethylene fuel.

| Parameter | Fuel Condition 1 | | Fuel Condition 2 | | Uncertainty |
|-----------------------|------------------|---------------|------------------|---------------|-------------|
| | Cavity-Side | Opposite-Side | Cavity-Side | Opposite-Side | |
| Equivalence ratio | 0.20 | 0.20 | 0.17 | 0.17 | $\pm 5\%$ |
| Total pressure (kPa) | 260 | 270 | 207 | 223 | $\pm 3\%$ |
| Total temperature (K) | 288 | 288 | 288 | 288 | $\pm 3\%$ |
| Mach number* | 1.0 | 1.0 | 1.0 | 1.0 | $\pm 0.5\%$ |

* Property at nozzle exit determined using nozzle area ratios and assuming isentropic flow ($\gamma=1.36$ for air, 1.24 for C_2H_4).

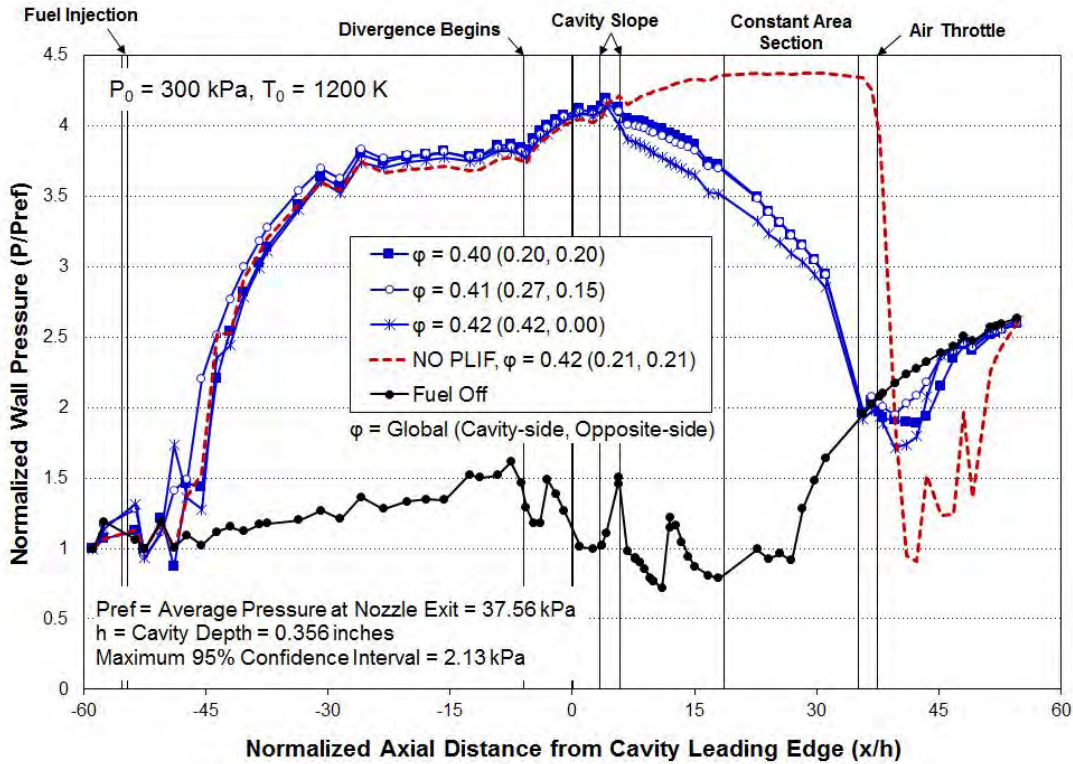


Figure 12. Normalized wall pressures at fuel condition 1. In the legend, the numbers in parentheses indicate the cavity-side and opposite-side fuel equivalence ratio, respectively.

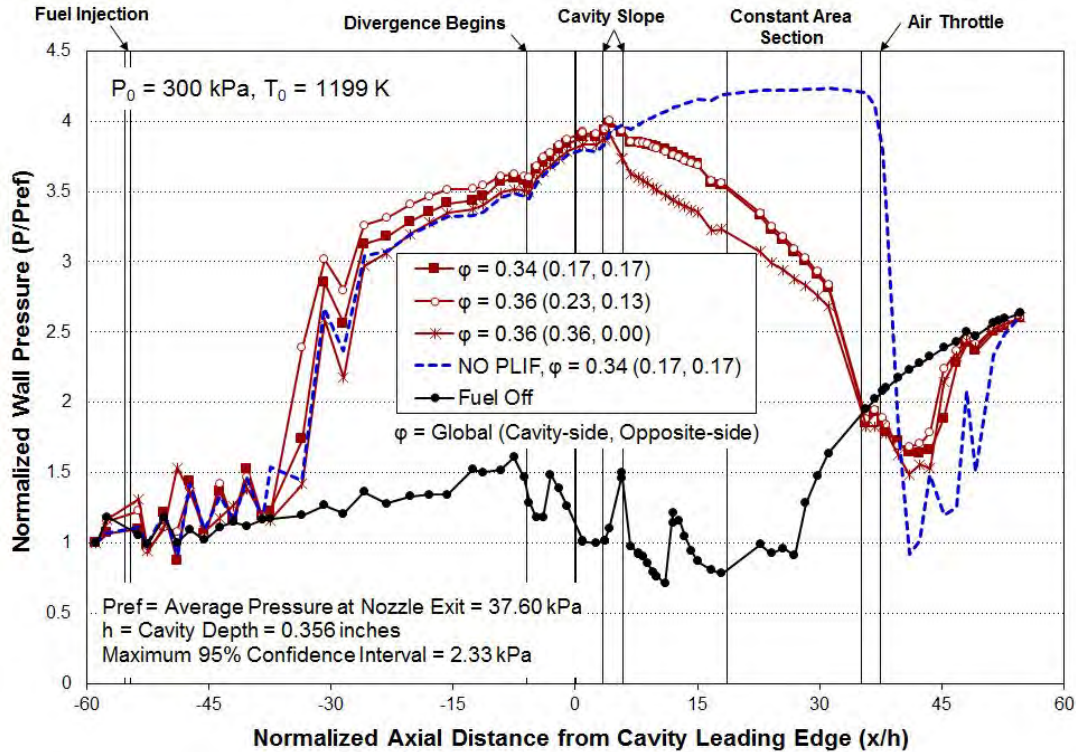


Figure 13. Normalized wall pressures at fuel condition 2. In the legend, the numbers in parentheses indicate the cavity-side and opposite-side fuel equivalence ratio, respectively.

4) Operability

It can be seen in Fig. 12 that the leading edge of the precombustion shock train approaches the isolator fuel injection location at global fuel equivalence ratios above 0.4. Impingement of the shock train on the fuel injectors results in ignition of the fuel in the isolator leading to a large pressure spike in the flowpath and likely damage or breakage of the windows. Thus, to provide some operating margin and avoid damaging tunnel hardware, a practical upper fueling limit for continuous testing is a global equivalence ratio of 0.42 with an absolute upper bound of 0.45.

In order to determine the lower flame holding limit, a number of lean and low temperature flameout tests were performed by slowly lowering either the fuel flow rate (lean flameout) or heater temperature (low temperature flameout) until the flame was no longer sustained. Figure 13 shows the results of these tests with each data point representing an observed flameout. Although there is some variability in the data, flameout consistently occurs at a global equivalence ratio just above 0.3 when the total temperature is 1200 K. Thus, the maximum range of equivalence ratio is about 0.14 or a little over 30%. At lower temperatures, between 1000 K and 1100 K, the fuel equivalence ratio required to sustain combustion rises to between 0.35 and 0.39 resulting in a range of operability of only 0.06 or 15%. Additional tests were performed with the air throttle on to provide additional back pressure such that the leading edge of the precombustion shock train was maintained at $x/h = -45$. At a total temperature of 1200 K, the incremental increase in static temperature behind the longer shock train sustains combustion down to an equivalence ratio between 0.26 and 0.29. This represents approximately 10% less fuel than with the air throttle off

and gives an operability range in equivalence ratio of 0.16 to 0.19, which is between 40% and 50%.

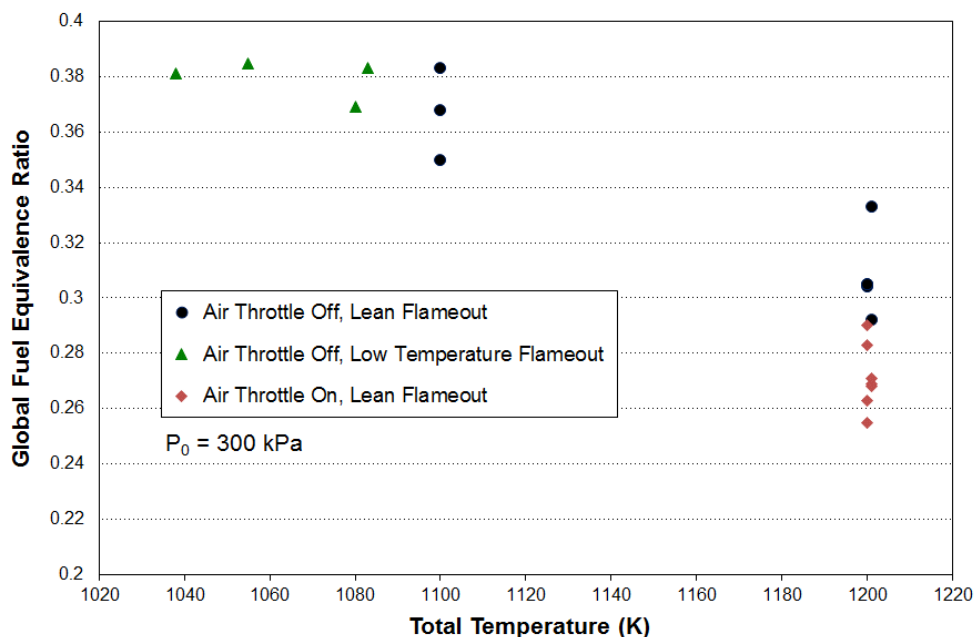


Figure 13. Lean and low temperature flameout points.

5) Chemiluminescence Imaging

Figure 14 is an instantaneous, high speed chemiluminescence image taken at a global equivalence ratio of 0.41 with approximately 2/3 of the fuel from the cavity-side injector bank and 1/3 from the opposite-side bank. Figure 15 is an image for the same setup taken at a global equivalence ratio of 0.31. The chemiluminescence is primarily due to emission from excited CH in the active reaction zone. Both images were taken with a 0.6 ms exposure. At both equivalence ratios, the flame is anchored on the cavity with combustion initiating along the shear layer between the cavity and the freestream air. The flame impinges on the sloped cavity closeout surface and propagates downstream, expanding away from the cavity-side wall. There is little to no chemiluminescence near the cavity leading edge in either case. As would be expected, the higher fuel rate results in a somewhat more robust and brighter flame. The field of view is limited to 6.6 cavity depths (2.35 inches) downstream of the cavity leading edge and at that point the flame propagates a little over halfway across the duct in Fig. 14 and little less than halfway in Fig. 15.

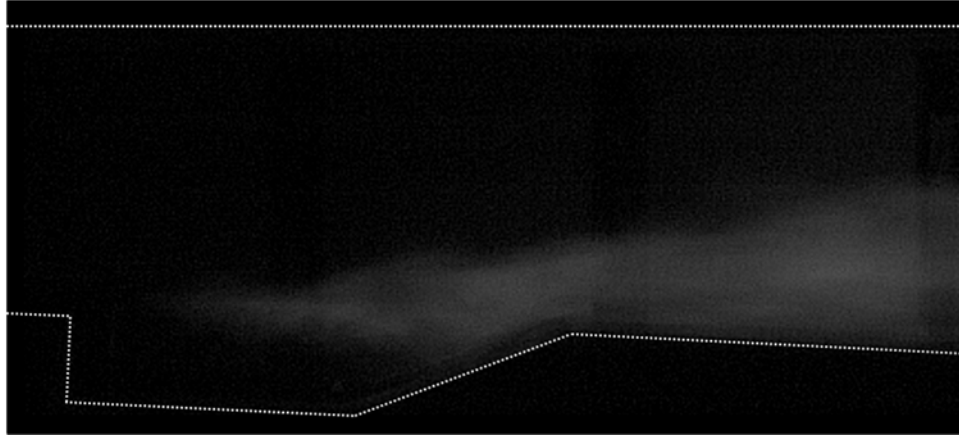


Figure 14. Chemiluminescence image (0.6 ms capture) at global $\phi = 0.41$ (cavity-side = 0.27, opposite-side = 0.15).

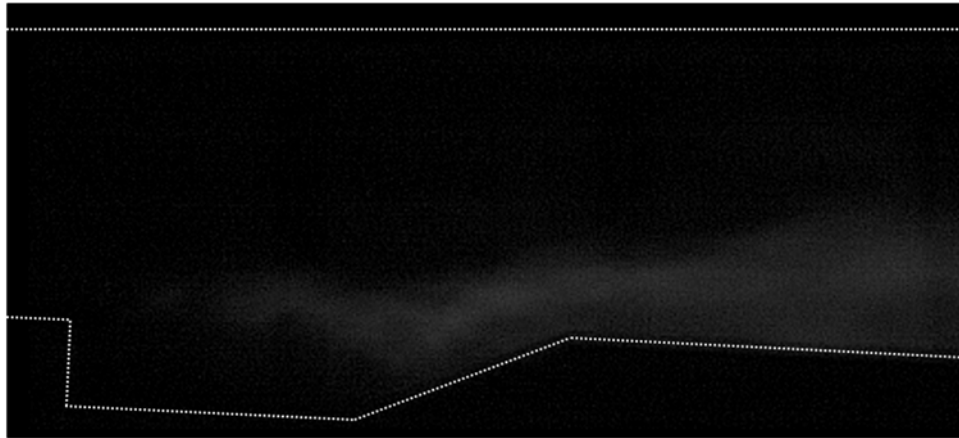


Figure 15. Chemiluminescence image (0.6 ms capture) at global $\phi = 0.31$ (cavity-side = 0.20, opposite-side = 0.11).

6) Mode Transition

Figure 16 shows a sequence of pressure scans taken at increasing global fuel equivalence ratios, which depict scramjet mode transition from the scram mode of combustion with no pre-combustion shock train to the dual-mode. In this test, the fuel was delivered through the primary fuel injectors on the cavity-side wall of the isolator as well as the secondary injectors immediately upstream of the cavity. The lower equivalence ratios (below 0.20) represent the scram mode of operation with no pressure rise upstream of the cavity and a one-dimensional Mach number of 1.62 at the cavity leading edge. Using a combination of the primary and secondary injectors in this fashion ensures some proportion of fuel-air premixing. However, the slope of the pressure curves in the combustor are more similar to that of the stratified fuel cases than the fully premixed cases in Figs. 12 and 13. Nevertheless, the data show that the facility and flow path are capable of supporting scramjet mode transition with ethylene fueling.

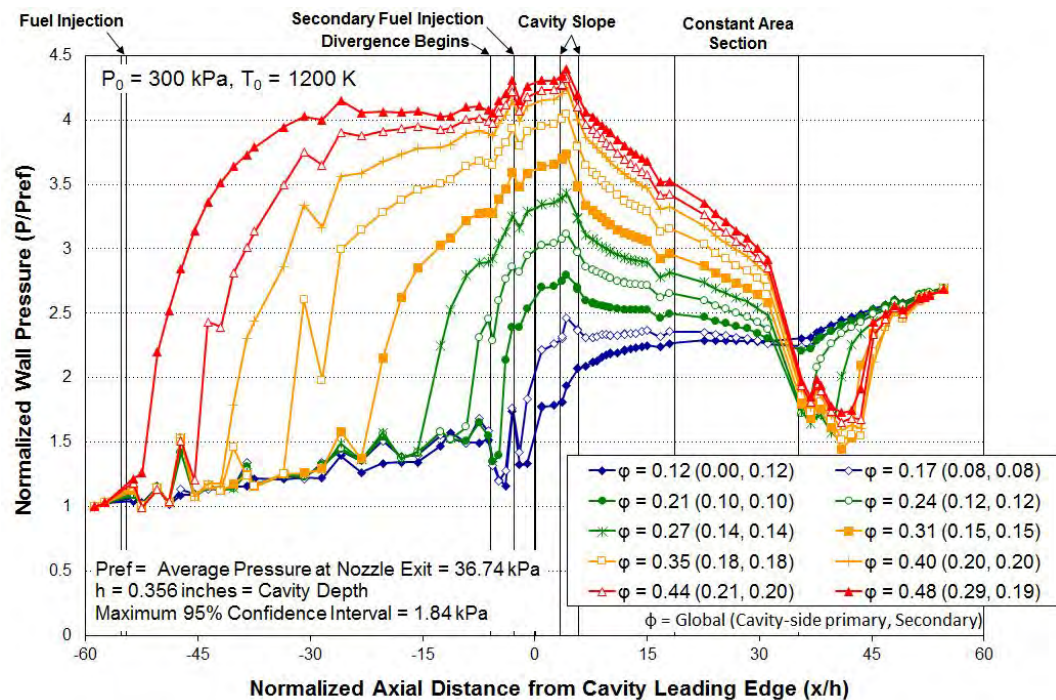


Figure 16. Normalized wall pressures illustrating mode transition with primary and secondary fuel injection. In the legend, the numbers in parentheses indicate the primary (cavity-side) and secondary fuel equivalence ratio, respectively.

Figure 17 shows the one-dimensional Mach number at the combustor entrance for the modified configuration E flow path with ethylene fueling as well as for the configuration C flow path with hydrogen fueling. The combustor entrance Mach number is calculated from the measured experimental pressure data using a Fanno flow model for the isolator upstream of the pre-combustion shock train and a separated flow model due to Heiser and Pratt for the pressure rise in the oblique shock train. The slightly higher entrance Mach number for the modified configuration E is due to the divergence in the flow path upstream of the cavity.

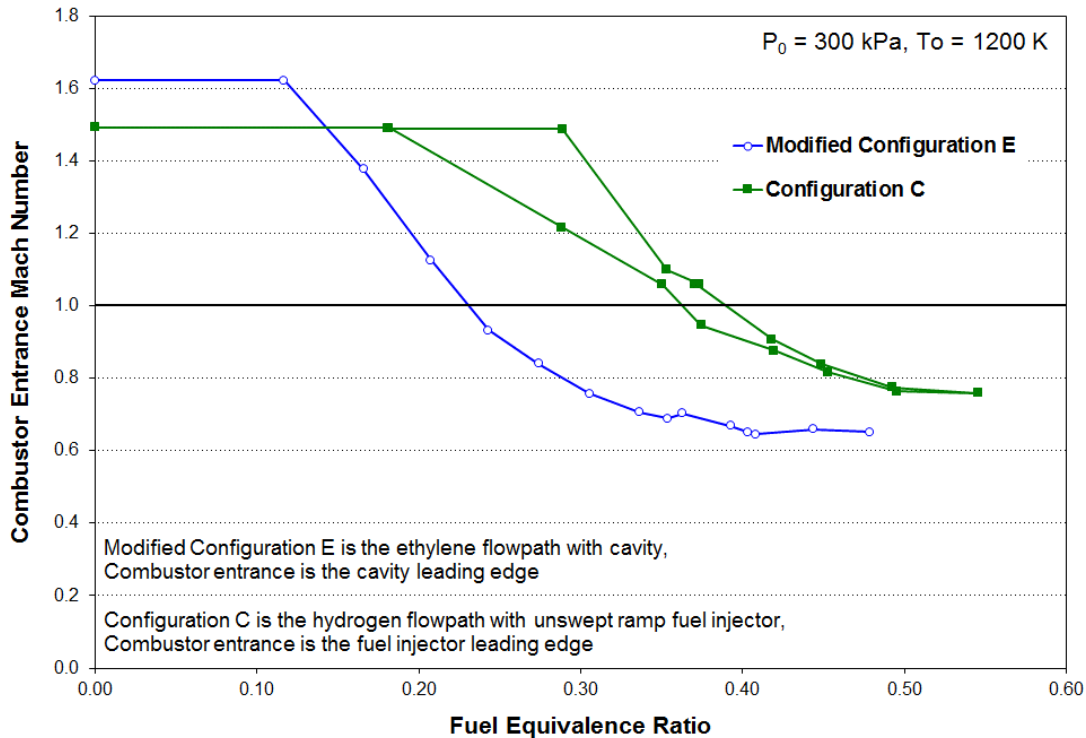


Figure 17. One-dimensional Mach number calculation

B. Numerical modeling of Premixed and Partially-Premixed Ethylene Combustion (Edwards)

Year 4 work focused on calculations performed for the Configuration E rig, in which the wedge-shaped flameholder used in Years 1-3 was replaced by a cavity. Ethylene fuel was injected through three banks of ports located just upstream of the flame, leading to a partially-premixed environment for ignition and flameholding. A mesh containing 65 M cells was used in these calculations. Experimental data for this configuration was limited to TDLAS profiles and wall pressure data. Ethylene oxidation was modeled using the Taitech-Princeton II reduced mechanism, which contains 22 species. Agreement with available TDLAS experimental data was generally good, though discrepancies in the amount of CO versus CO₂ produced in the cavity and the level of water production downstream of the cavity were present. The LES/RANS database was analyzed to produce an estimate of the cavity residence time (~0.0025 s). This estimate was in close agreement with that determined from monitoring the decay of the TDLAS cavity temperature signal during a blowout event. Analyses of the flame structure were performed using variants of the Takeno index to delineate lean premixed, rich premixed, and diffusion branches. The analysis revealed that rich premixed flame propagation occurs within the cavity and within the cavity shear layer. High strain rates lower flame temperatures near the cavity re-attachment point, but the flame remains connected, transitioning into a fuel-lean diffusion-flame structure further downstream. Comparisons of the calculated flame angle with that obtained using classical turbulent flame-speed estimates were favorable, indicating that such theories qualitatively hold even in the high turbulence intensity environment of the Configuration E rig.

Computational work performed during Year 5 focused on the development of methods to premix ethylene fuel and air at the combustor entrance plane and on the simulation of premixed combustion within the experimental ring using large-eddy simulation / Reynolds-averaged Navier-Stokes (LES/RANS). Many RANS simulations were performed to determine injector placement and operating conditions that led to optimal fuel-air mixing within the operability constraints of the UVa facility (equivalence ratio (ER) $< \sim 0.45$). The primary result was that uniform fuel-air mixing could be achieved if fuel was injected at the beginning of the isolator and if a shock train was present in the isolator. Processing of the fuel plume via a system of shock waves leads to vorticity generation through baroclinic torque effects. This, along with enhanced turbulence levels due to multiple shock / boundary layer interactions, facilitates near complete mixing at the combustor entrance plane.

Reactive LES/RANS simulations were then conducted for one case (ER ~ 0.42) designated for a detailed flow mapping using SPIV, CARS, and OH/CH₂O imaging. The Taitech-Princeton 22-species reduced mechanism for ethylene-air combustion was employed, as were various strategies for reducing numerical dissipation in the simulations. Inflow turbulence-generation methods were not used, as the shock train facilitates the natural evolution of large-scale turbulence in the isolator. The calculations were performed on a mesh containing ~ 93 million cells, designed so that the mesh spacing away from solid walls was ~ 0.25 mm – fine enough to ‘capture’ a premixed flame front (including the pre-heat zone) but not fine enough to resolve the inner structure of a premixed flame in great detail. The results show that a premixed flame is anchored within the cavity and that the flame propagates into the core of the combustor. The combustor response is characterized by an oscillation in heat release and average combustor pressure level with a period of oscillation of about 2.8 ms (357 Hz). The flame angle varies significantly over the cycle (see average and instantaneous temperature contours in Figure 18). Maximal heat release corresponds to a shallower flame angle, an increased flame surface area, and increased core flow velocities. Minimal heat release corresponds to a steeper flame angle, decreased flame surface area, and reduced core flow velocities. The reduction in core-flow velocity is a consequence of the upstream propagation of a normal shock within the isolator. Raw wall pressure distributions (Figure 19, left), illustrate the high degree of cyclic variation in the isolator and combustor. Conditionally-averaged wall pressure distributions based on heat release (Figure 19, right) show variations in the shock structure that lead to the cyclic response.

Flame-angle predictions using Zimont’s estimate of the turbulent flame speed are in good agreement with computational time-averaged images. (Figure 20) The flame itself is stabilized at a position about two-thirds along the cavity length, near the point where the ramp begins to close the cavity. The region upstream of the stabilization location is associated with high concentrations of major product species and lower temperatures; this region acts as an ignition source for freshly-entrained premixed fluid. Cavity streamline patterns and residence-time estimates in Figure 21 indicate significant differences between the current dual-mode case and a previously-computed scram-mode case with fuel injection just upstream of the cavity. The most probable residence time is ~ 10 ms for the dual mode case, compared with ~ 2.5 ms for the scram-mode case considered in Year 4. This shows why dual-mode operation is favorable for flame stabilization.

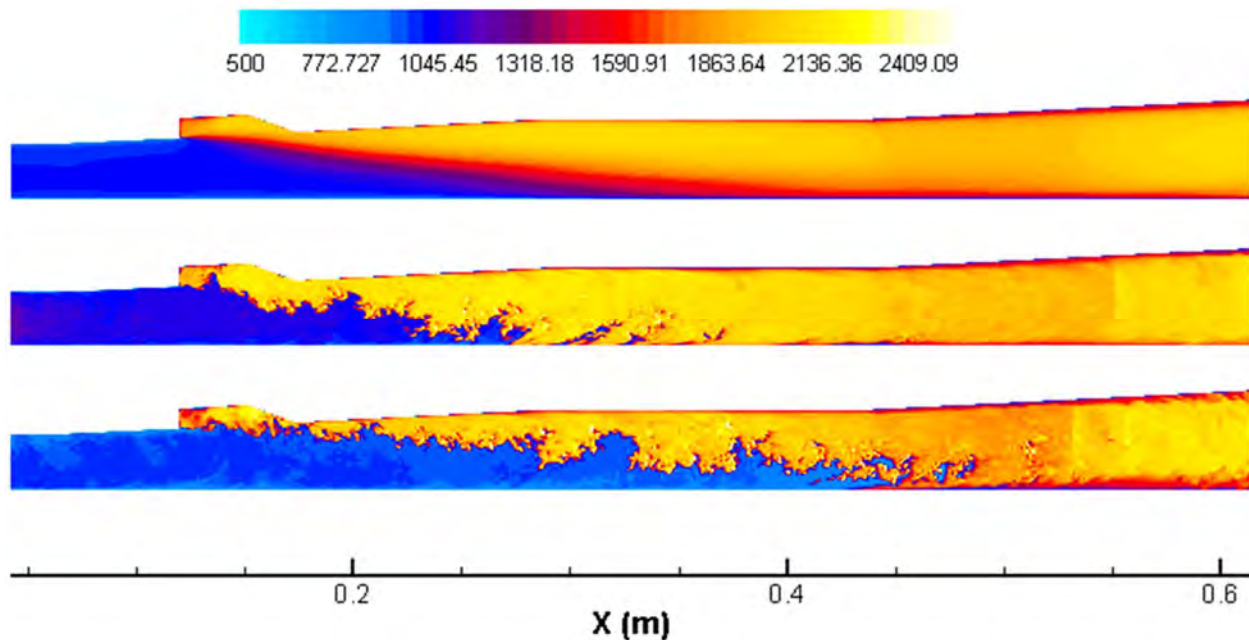


Figure 18: Temperature contours (top: average; middle: minimum heat release; bottom: maximum heat release)

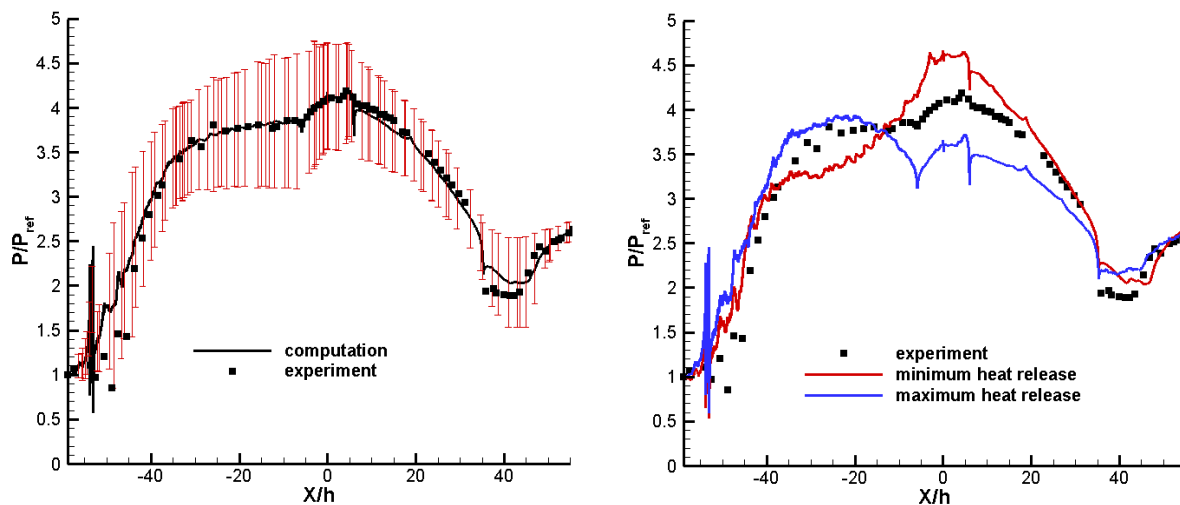


Figure 19: Left: raw wall pressure distributions with one standard deviation in pressure fluctuations shown as 'error bars'; Right: wall pressure conditionally averaged based on heat release

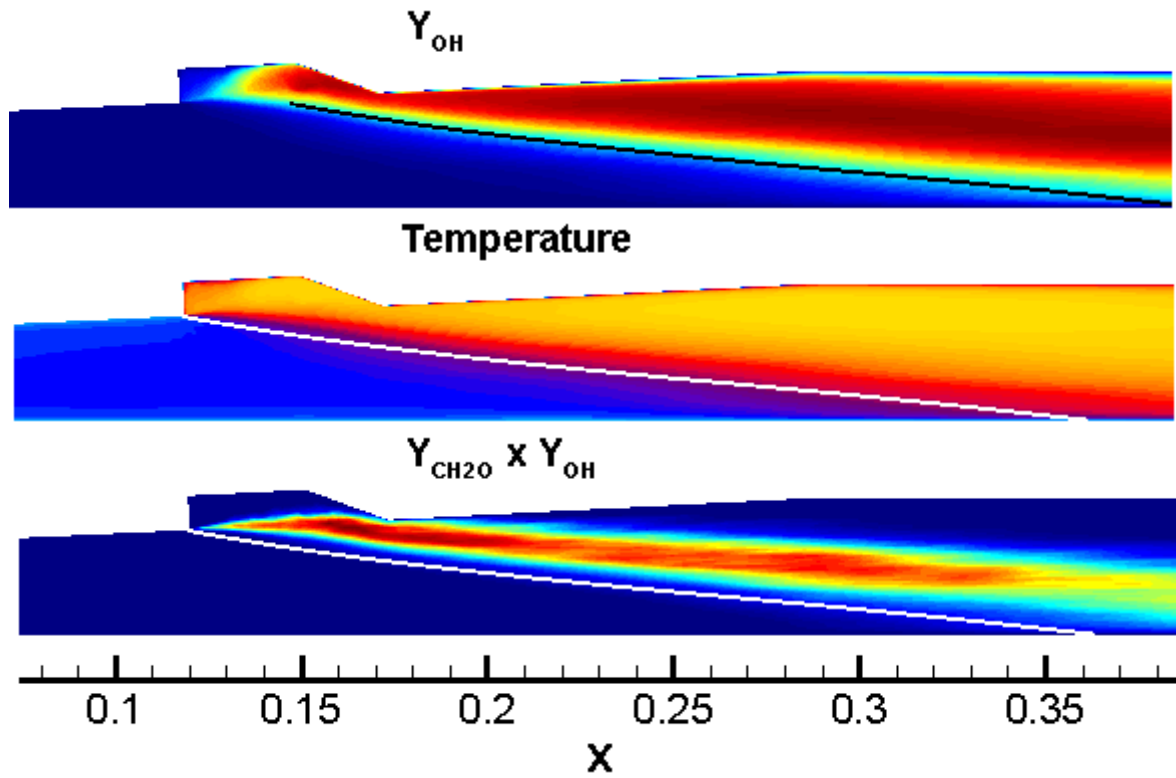


Figure 20: Flame angle predictions (white lines) versus time-averaged data

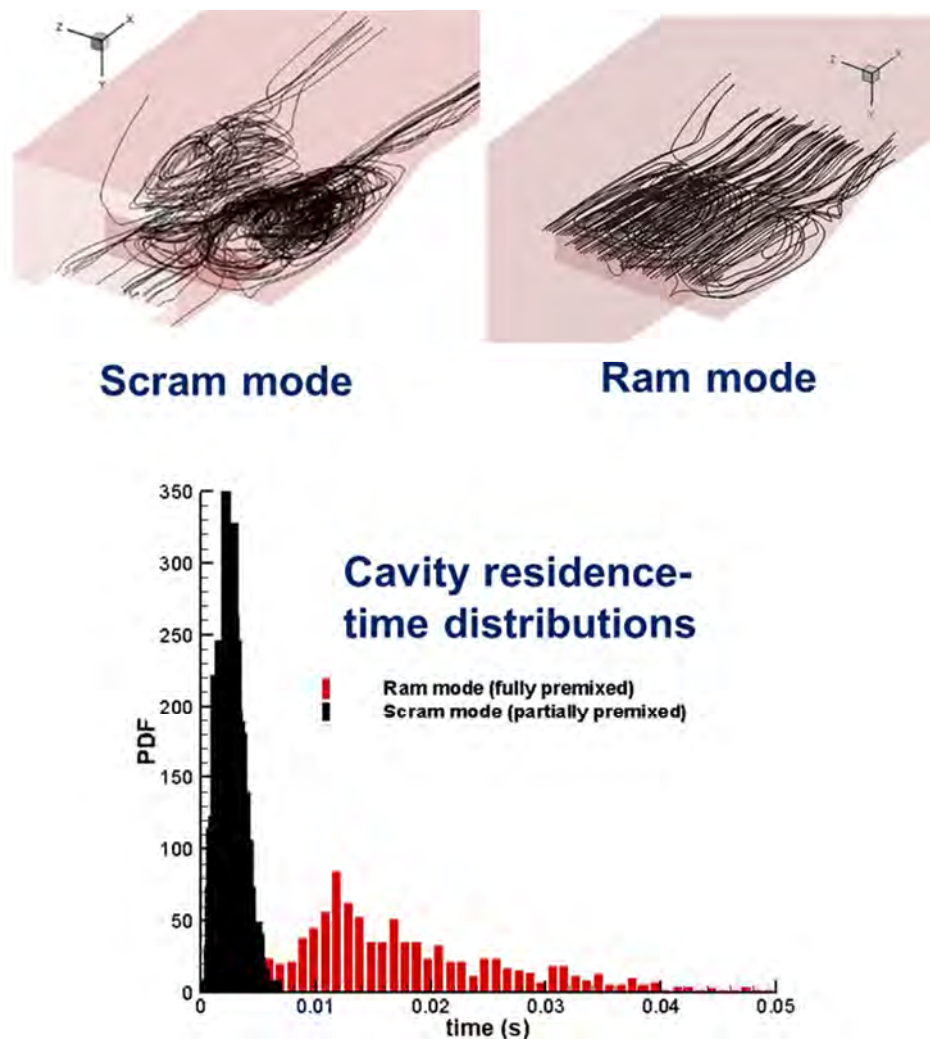


Figure 21: Cavity streamline patterns and residence time distributions for ram-mode and scram-mode operation

C. Diagnostics

a. CARS, OH PLIF and NO PLIF (Cutler)

Semi-quantitative NO PLIF imaging techniques and the WIDECARS technique for simultaneous spatially and temporally resolved measurement of flow temperature and mole fractions of N_2 , O_2 , H_2 , CO_2 , CO , and C_2H_4 were developed. Additional CARS spectral fitting software was developed to allow simultaneous fitting of the larger number of chemical species. The PLIF-CARS system was transported to UVA for a final lengthy test campaign. Extensive data bases of several types were acquired in (modified) Configuration E. This is an ethylene fueled, cavity stabilized flame combustor with long inlet isolator. Fuel is injected near the upstream end of the isolator and fully mixed with the air at the flame front. Non-combusting fuel-air mixing studies were performed, along with combustion studies varying fuel-air equivalence ratio and facility air temperature.

This test campaign was completed in November 2014. Because of the intensive nature of the campaign the data could not be fully analyzed during the test campaign. Indeed CARS data spectral analysis is very laborious (250,000+ spectra were acquired in the UVa scramjet). This PLIF and CARS data analysis is continuing and the results will form the PhD dissertations of Luca Cantu and Emanuela Gallo (GW students who expect to complete their PhD's by summer 2015.) It is anticipated that data analysis and writeup will be complete at that time, though publication at conferences and in journals will continue.

The experiments/databases involved and findings associated with them are as follows:

NO-PLIF: Simulated fuel-air mixing studies were performed to establish the state of mixing of fuel at the beginning of the cavity. The fuel (ethylene) was simulated by a mixture of NO (10%) and N₂, which has almost the same molecular weight as ethylene. A theoretical study of the selected NO rotational transitions was performed to obtain a LIF signal that is linear with NO mole fraction and approximately independent of pressure and temperature. Fuel relative mole fraction images were acquired at the entrance plane to the combustor. This work has been presented at an AIAA conference. Additional NO PLIF studies were performed of the mixing of NO injected into the cavity to study mass exchange between the cavity and the freestream, which will be published in the context of the OH-PLIF imaging.

This method was used to screen different possible fueling configurations to provide optimized test conditions for follow-on combustion experiments using ethylene fuel. In the NO-PLIF experiments, the pressure distribution in the inlet isolator was matched to the cases with combustion by use of an air throttle located downstream of the combustor section in the "extender". The air throttle choked the flow downstream, raising the pressure in the same way that combustion does, and forcing a shock train into the isolator. The shock train leading edge could be adjusted in this way to match any desired combustion condition. *An injector configuration and range of operating conditions (attainable with combustion) was identified where the mixing was perfect* (i.e., produced uniform fuel-air composition within measurement precision). Flush wall injectors were located near the upstream end of the isolator injected fuel symmetrically from both sides of the flow, and the combustion-induced shock train (which significantly enhances the mixing) with leading edge was located close downstream to the injectors, where it would occur due to combustion at the simulated fuel-air equivalence ratio. The nominal equivalence ratio was in the range 0.3 to 0.4.

Figure 22 shows some typical NO-PLIF results. The single-shot image of the fuel plume produced by a single flush-wall injector located near the upstream end of the inlet isolator is shown in Fig. 22(a), while the uniform distribution produced in the final premixed configuration is shown in Fig. 22(b). (The left to right variation is due to absorption of the laser light sheet, which propagates left to right, and reduces the energy locally available for absorption and emission as fluorescence.)

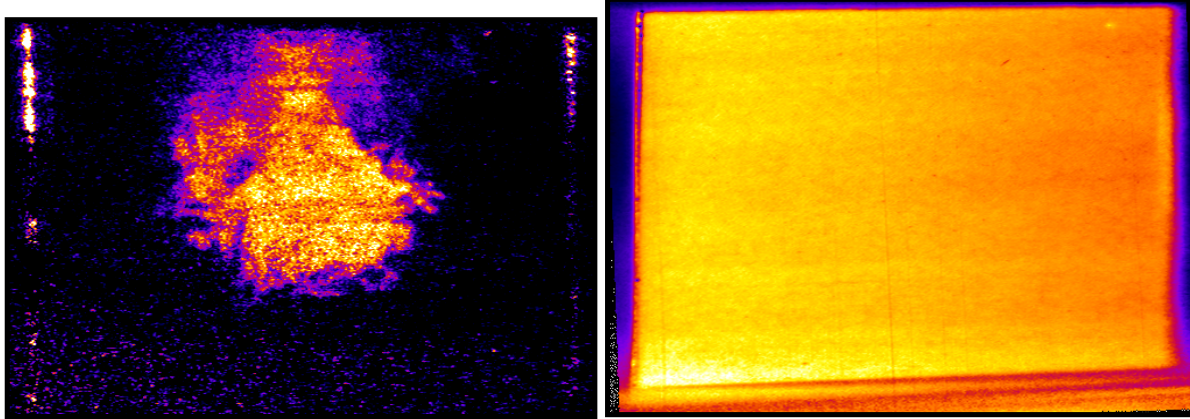


Figure 22: Typical NO-PLIF images (a) single laser shot, single fuel injector; (b) final configuration.

OH-PLIF: Extensive imaging of OH in multiple planes in the vicinity of and downstream of the cavity was performed in the combustor cases. These results are in process of being analyzed, including data processing to correct for experimental effects such as background signal and laser non-uniformity, and image analysis to extract combustion science information such as flame angles, flame intermittency, flame surface area, etc. Data will be published and shared with the computational modelers when available.

Figures 23 and 24 show preliminary results for the OH-PLIF imaging at the baseline operating condition. The propagation of the flame is illustrated by composites of three images obtained in the streamwise symmetry plane of the combustor and stitched together (Fig. 23). Figure 23(a) is based on three single shots, obtained at different times and selected to roughly match where joined. Figure 23(b) is based on three mean images. An instantaneous and a mean image in a spanwise plane just downstream of the end of the cavity closeout ramp (coinciding with CARS measurement plane 3) are shown in Fig. 24. Some preliminary findings from the PLIF pertaining to the cavity-stabilized premixed experiments include the following:

- The flame is stabilized on the cavity leading edge and propagates (in the downstream direction towards the opposite wall (Fig. 23).
- The flame is two-dimensional, with only minor side-wall effects (Fig. 24.)
- The flame angle varies little with equivalence ratio and facility stagnation temperature from the baseline operating conditions (nominal fuel-air equivalence ratio $\phi = 0.4$ and stagnation temperature $T_t = 1200\text{K}$) to near blowoff conditions ($\phi = 0.4$, $T_t = 1100\text{K}$ and $\phi = 0.33$, $T_t = 1200\text{K}$)
- When NO is seeded into the cavity instead of into the fuel in non-combusting cases (with back-pressure by the air throttle to match the combustion case), the NO-PLIF images are very similar to the OH-PLIF with combustion
- Consequently, the flame propagation (angle) seems to be through the diffusion of radicals and energy by the *preexisting* inflow freestream turbulence.

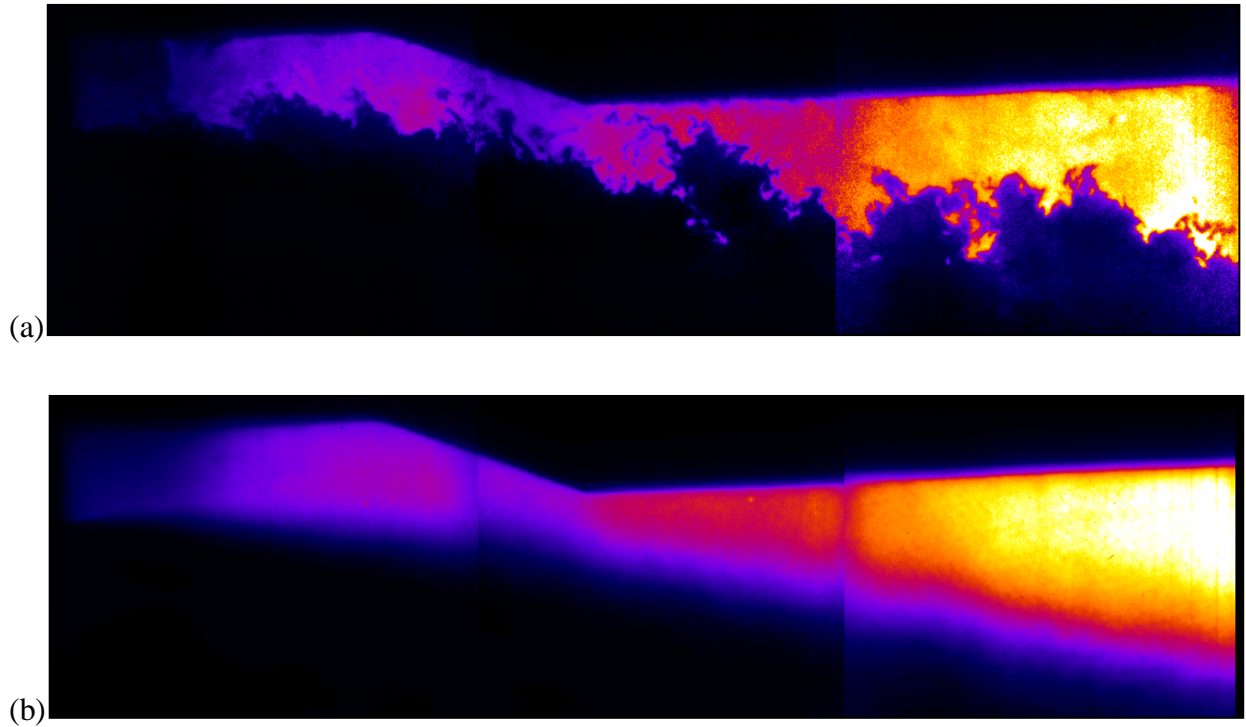


Figure 23: Composite of three OH-PLIF images in the streamwise symmetry plane stitched together: (a) single shots, (b) averages

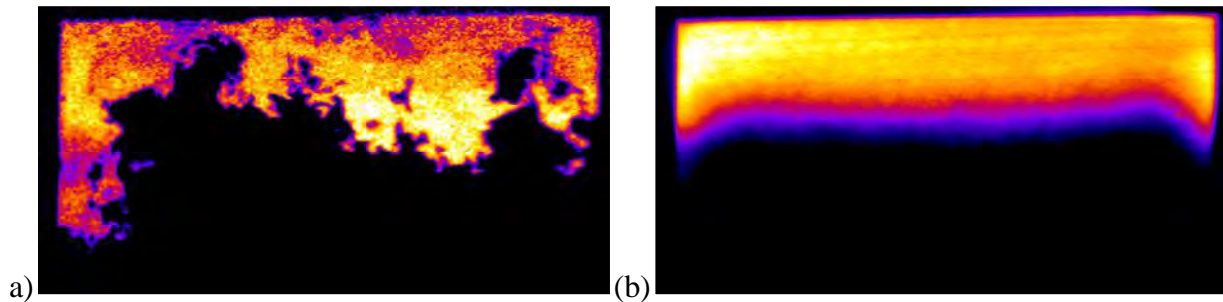


Figure 24: OH-PLIF images in the spanwise direction at a location corresponding to CARS plane 3: (a) single shot, (b) average.

WIDECARS: Developmental work for this technique, along with measurements acquired in premixed fuel-lean and fuel-rich (including sooting) flames above a McKenna burner (acquired at NASA Langley) has been published, and a paper on the spectral fitting techniques will be presented at a summer 2015 AIAA meeting. Additional measurements in this burner were acquired at UVa in the setup at the scramjet; this more recent data has been analyzed but not yet published. Good agreement was found between the WIDECARS McKenna burner measurements of temperature when compared to results from the literature. In a lean flame, comparison of measured product composition with composition calculated assuming chemical equilibrium was good. In a rich flame, chemical equilibrium is not a good assumption, especially as the sooting condition is

approached. Concentration results are plausible in the fuel-rich cases, but good calculations of the variation of properties through the flame are still being sought for comparison with CARS flame surveys. [Note that the scramjet application is premixed at uniform fuel-lean conditions, so not an issue there.] Figure 25(a) shows WIDECARS measurements of temperature in a scan through the $\phi = 2.1$ sooting flame, and comparisons to CARS measurements and simulations by Bladh et al., showing good agreement. Figure 25(b) shows comparisons of WIDECARS temperature with measurements by Vestin et al 1 cm above the surface of the McKenna burner as equivalence ratio ϕ is varied, again showing good agreement.

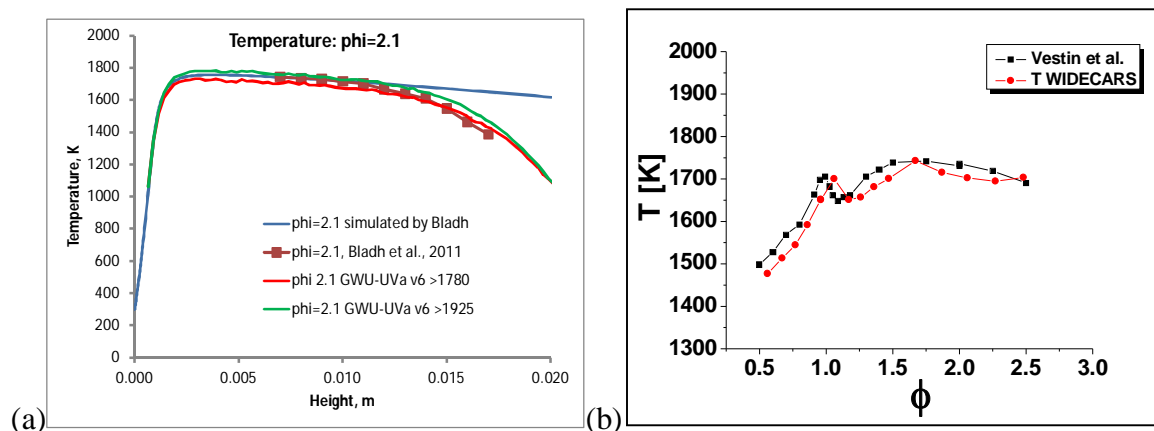


Figure 25. WIDECARS temperature measurements in the McKenna burner: (a) scan just above the surface in a $\phi = 2.1$ sooting flame; (b) 1 cm above the surface as ϕ is varied.

Extensive mapping with the WIDECARS technique was performed in the scramjet. Measurements are at four streamwise locations (CARS planes 1, 2, 3, 4): plane 1 is near the combustor entrance, plane 2 is near mid cavity, plane 3 just after the end of the cavity closeout ramp, and plane 4 is near the downstream end of the PLIF view in Fig. 23. This data are in the process of being analyzed. The single shot measurements are being analyzed to obtain statistics (such as means, variances, covariances, etc.) of the measured parameters of the flow (temperature and mole fractions), as well as conditional statistics (based on presence of flame or not), and histograms, etc. Results for various cases will be compared to each other as well as canonical measurements in low speed (low Reynolds number) turbulent premixed flames from the literature. Data will be shared with the modelers as soon as available.

Figure 26 are some results of preliminary fitting of averaged WIDECARS spectra (the data processing work of fitting averages is much less than of fitting single shots and averaging the results, since there are so many more single shots, but there are inaccuracies inherent in this method and it does not provide statistical information on the fluctuations.) Plots of temperature and mole fraction species at the streamwise symmetry plane of the scramjet (baseline operating conditions) in a direction perpendicular to the observation wall (the wall opposing the cavity) are shown. Positive y is oriented towards the cavity. Results show a rise in temperature and products species (CO_2) coincident with a drop of O_2 as the cavity-side wall is approached, and streamwise growth of the combustion region, as expected.

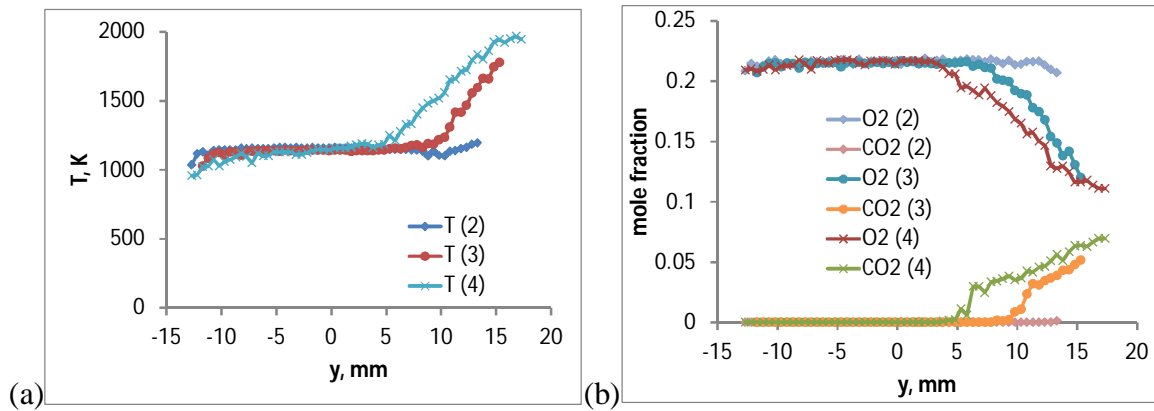


Figure 26. WIDECARS surveys of (a) temperature and (b) mole fraction species (b) at CARS planes 2, 3, 4, on the streamwise symmetry plane.

Other preliminary findings and observations follow:

- The WIDECARS technique was successfully applied to a supersonic combustor flow, with the first ever simultaneous measurements (and extensive mapping) of temporally and spatially-resolved temperature and mole fraction multiple species in a hydrocarbon-fueled scramjet.
- Temperature and mole fraction N_2 , O_2 , CO_2 could be satisfactorily measured on a single-shot basis. CO was detected at close to the measurement threshold for detection (0.01-0.02 mole fraction). No H_2 was detected (except during the process in which the flame in the scramjet is initiated, which uses a temporary flow of H_2 .)

b. kHz-rate PIV (Goyne)

A kHz-rate PIV system was used to measure velocity along the streamwise symmetry plane of the cavity flameholder in the direct-connect scramjet flowpath (non-combusting experiment). As an example of the data collected, Fig. 27 presents contours of mean velocity with overlaid pathlines, generated via an ensemble average of 1971 image pairs. A multi-pass post-processing scheme was used to achieve a final spatial resolution of two vectors per millimeter, and vector count at all locations exceeds 1700. The total temperature of the flow was 1200 K, and fuel injection was simulated via injection of gaseous nitrogen in the flowpath isolator at a molar flow rate corresponding to ethylene combustion at an equivalence ratio of 0.42. A distinct pattern of recirculation is observed, through which mass and momentum are exchanged between the high-velocity freestream and low-velocity cavity interior. This experiment included the first use of graphite flakes as a tracer material in a high-speed flow, which eliminated the problem of tracer adhesion to facility windows encountered when using titanium dioxide or silicon dioxide.

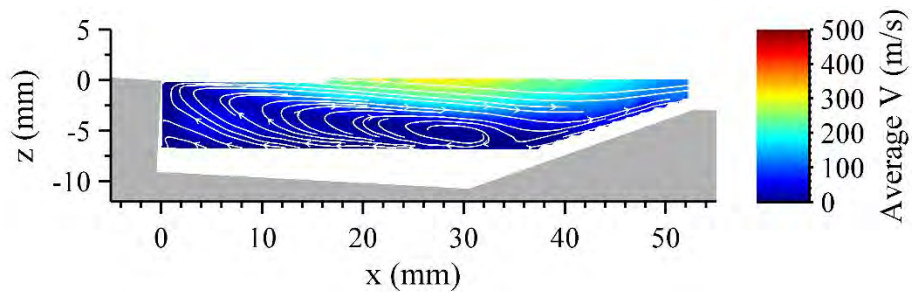


Figure 27: kHz PIV data in cavity using graphite particle tracers

c. kHz PLIF: OSU (Lempert and Sutton)

One target of the experimental campaign at UVa was high-speed imaging using optical and laser diagnostics to study the flame dynamics in a cavity-stabilized premixed, ethylene-fueled dual-mode scramjet combustor. High-speed imaging of CH^* chemiluminescence was used to observe global flame dynamics, while high-speed (50-kHz acquisition rate) CH_2O PLIF imaging was developed with the goal to track flame structure as a function of space time. In order to facilitate CH_2O PLIF imaging at 50 kHz, modifications to an existing pulse burst laser system were performed including the addition of a new pulsed fiber laser master oscillator. Following optimization, output energies of 40 mJ/pulse at 355 nm at 50 kHz were achieved. Measurements at UVa consisted of 5 to 50 kHz CH^* imaging at an operating condition of $\phi = 0.42$. From these measurements, information regarding the flame anchoring position (in the axial direction) and flame spreading angle is collected, providing insight on the effect of cavity flame-holding and flame penetration into the freestream flow. 50-kHz CH_2O measurements were acquired in the spanwise direction. Measurements in the axial flow plane were not possible due to significant interference from laser light scattering and fluorescence resulting from the laser sheet impingement on the cavity floor. During the measurements a “hot spot” developed within the pulse burst output beam, resulting in an intense non-uniform intensity distribution and damage to many optical components. To correct this output would require significant system alignment/optimization which could not be performed either onsite at UVa or within the remaining timeframe of the experimental program. In this manner a decision was made to shift to “low” repetition-rate (10-Hz) measurements using a “commercial” pulsed Nd:YAG laser with high beam quality at several cross-flow planes in order to build up a statistical description of the flame structure. This approach allows the determination of low-order statistics such as the mean and RMS of the CH_2O topology such that axial reconstructions of the entire span-wise CH_2O field can be performed. For axial flow positions upstream of the trailing edge of the cavity, CH_2O was highly intermittent and sparsely detected. For axial position downstream of the trailing edge of the cavity, CH_2O structures were present in the majority of images acquired and appeared to be at a maximum near the walls and windows. Initial results indicate that, when present, the CH_2O structures are highly wrinkled and contorted, but are somewhat “thin”, meaning that their width (in the spanwise direction) is much greater than their thickness. More specifically, the CH_2O topology does not resemble that which would be expected from a “well-stirred” or “partially-stirred” reactor, but clearly show distinct structure.

D. Chemistry modeling (Chelliah)

1. Finite-Rate Chemical Kinetics and Thermal Choking Analyses of Premixed Ethylene-Air Mixtures under UVa Facility Operating Conditions

1.1 Ignition delay time analysis

Cavity or recirculation regions are critical for stabilization in high-speed premixed reacting flows owing to very short residence times, typically of the order of 0.2 ms. To illustrate this point, Fig. 28 shows the typical ignition delay times of ethylene-air mixtures (equivalence ratios from 0.1 to 0.9) at the vicinity of the cavity (without mixing of partially reacted species from the cavity). Here, the ignition delay values were calculated using a C0-C4 sub-mechanism of the JetSurf2.0 kinetic model and the ignition delay times in present zero-dimensional simulations were defined by the inflection point of temperature profile corresponding to maximum heat release rate. For the scramjet operational condition of the facility ($M=2$) with the local static temperature of 677 K and static pressure of 0.3 atm (identified as A1 condition), Fig. 28 indicates an ignition delay time is of the order of 100 s or greater, far exceeding the local flow residence time and confirming the need for flame stabilization mechanism in the form of a cavity or a recirculation region.

Even for the ramjet operating conditions of the UVa facility with a higher local static temperature of 1125 K and static pressure of 1.7 atm, corresponding to a Mach number of 0.577 (identified as A2 condition), the predicted ignition delay time still remains several factors greater than the local flow residence time over the cavity (see Fig. 29). Furthermore, if one consider the uncertainties associated with chemical kinetic models, at 1125 K it is very unlikely that the ignition delay time of ethylene-air mixture with an equivalence ratio of 0.4 (upper limit at UVa facility based on thermal choking considerations) will drop below the local flow residence time. In this regard, it is clear that mixing between the partially oxidized species from the cavity and the main flow of ethylene-air is essential to reduce the ignition delay time to values below 0.2 ms and achieve successful flame holding.

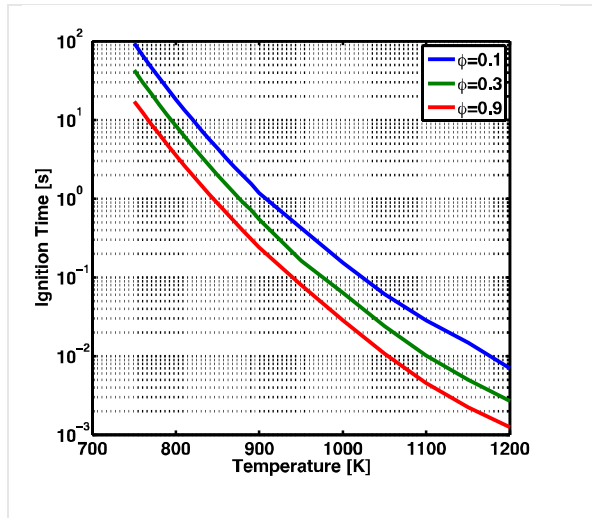


Figure 28: Predicted ignition delay time of ethylene-air mixtures near scramjet operational conditions ($M=2$, $p=0.3$ atm).

The CFD simulations have indicated that the typical cavity residence times are of the order of 2 ms. This information, together with mass flux rate between the cavity and the main flow can be used to construct a simple phenomenological model to illustrate the cavity effects on flame holding. An illustration of the one of the conceptual model used in this analysis is shown in Fig. 30, consisting of a perfectly stirred reactor (PSR) representing the cavity followed by instantaneous mixing between the cavity and the main flow leading to ignition. In the PSR model, the residence time was set to 2 ms with composition, temperature, and pressure same as the main flow. Since mass flux rate or exchange rate between the cavity and the main flow was not available, a series of mass exchange rates were assumed in estimating the effects of radicals and combustion products from cavity on flame holding. Figure 31 shows an example of such calculations showing that 1-5% mass exchange rate can reduce the ignition delay time to 0.2 ms, same as the flow residence time.

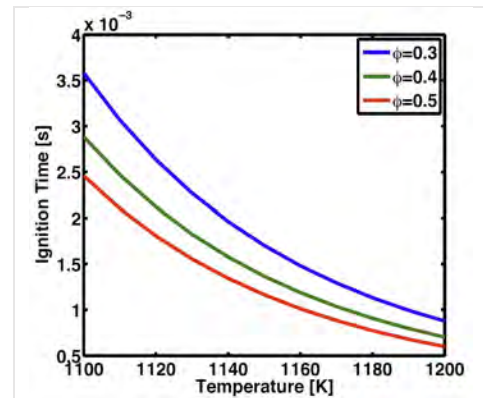


Figure 29: Predicted ignition delay time of ethylene-air mixtures near ramjet operational conditions ($M=0.577$, $p=1.7$ atm).

A variation of the conceptual mixing arrangement in the phenomenological model was considered by replacing the zero-dimensional induction module by a partially-stirred reactor model to better understand the coupling between finite-rate kinetics and mixing.

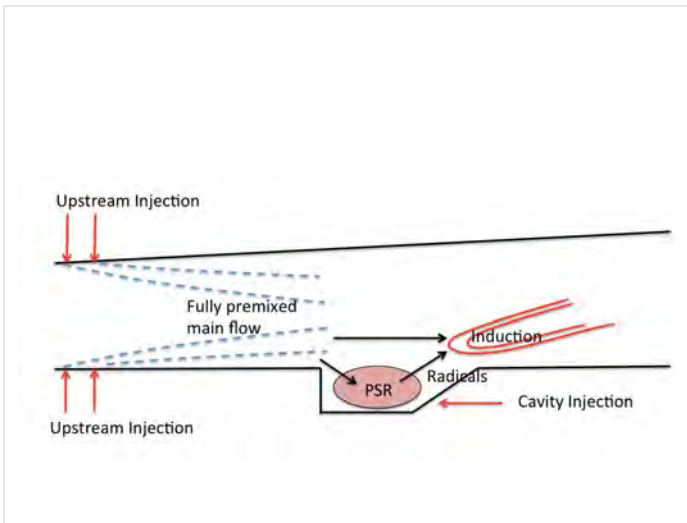


Figure 30: A conceptual model showing the cavity reaction represented by PSR model and the mixture of main and cavity reaction represented by a zero-dimensional ignition model.

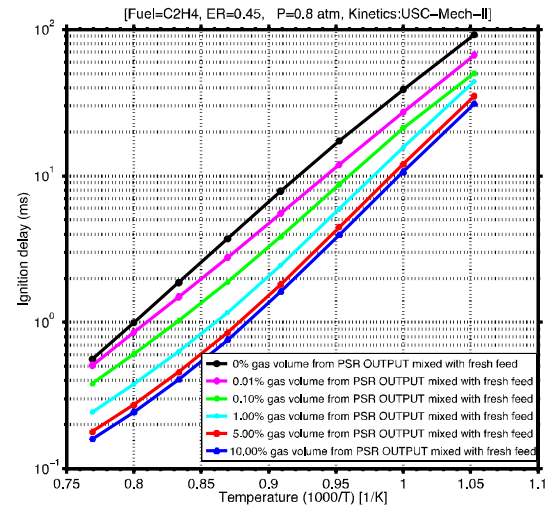


Figure 31: The effect of mass exchange rate between the cavity and the main flow on overall ignition delay time.

1.2 Premixed Burning Velocity Calculations

For fully premixed conditions at the leading edge of the cavity, to understand whether any portion of the flame front corresponds to a truly premixed flame, a series of laminar burning velocity or flame speed calculations were performed under the local composition, static temperature and pressure conditions. The basic premise here was that calculated laminar burning velocity and the experimentally observed flame angle can be used to obtain an accurate estimate for the ratio of turbulent burning velocity to laminar burning velocity. Such a ratio can also be used to estimate the local turbulent velocity, which can be verified by experiments or simulations.

Figure 32 shows calculated ethylene-air burning velocities for conditions A1 (scramjet) and A2 (ramjet) with a M=2 nozzle. For example, use of A2 burning

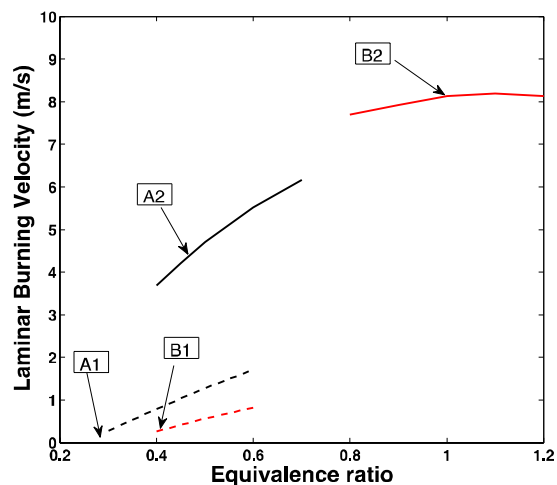


Figure 32: Laminar burning velocity of ethylene-air mixtures for scramjet conditions (A1) and ramjet conditions (A2), using JetSurf2.0 model.

velocity with experimentally observed mean flame angle yields a ratio for S_T/S_L of about 22, which is realizable in these highly turbulent flows.

1.3 Thermal Choking Limits of UVa Facility

The upper equivalence ratio limit of the UVa supersonic combustion facility is constrained by thermal choking effects. A quasi one-dimensional model with realistic pressure variation in the diverging section and heat release effects was developed to assess these limits. The key assumptions imposed in deriving the model were: (i) pressure varies linearly in the diverging reacting flow section (supported by experimental evidence) and (ii) heat release occurs over the entire length of reacting flow section (from leading edge of the cavity to the thermal choking point). By integrating the mass, momentum, and energy equation, for given initial total temperature, T_{01} , Mach number, M_1 , and $M_2=1$, the solution of the following two equations:

$$q = c_p(T_{0,2} - T_{0,1})$$

$$\frac{T_{02}}{T_{01}} = \left(\left(\frac{M_2}{M_1} \right) \frac{\gamma M_1^2 + 0.5(1 + \frac{A_2}{A_1})}{\gamma M_2^2 + 0.5(1 + \frac{A_1}{A_2})} \right)^2 \left(\frac{1 + \frac{\gamma-1}{2} M_2^2}{1 + \frac{\gamma-1}{2} M_1^2} \right)$$

yields values of A_2/A_1 as a function of the equivalence ratio, ϕ . In Eq. (1), the equivalence ratio determines the value of q , thus the ratio of T_{02}/T_{01} .

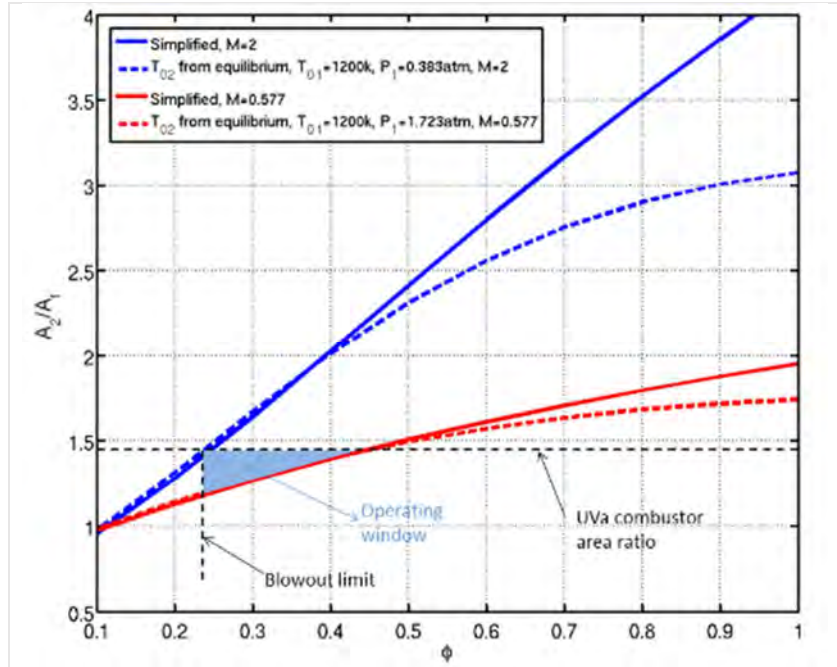


Figure 33: Plot of area ratio vs equivalence ratio (ϕ) yielding thermal choking conditions, for scramjet case (blue lines) and ramjet case (red lines). The solid lines are for product species without dissociation and dashed lines are with dissociation.

For $T_{01}=1200$ K and $M_1=2$ nozzle, Figure 33 shows the estimated area ratio where choking happens as a function of equivalence ratio, for two operating conditions, i.e. scramjet (A1) and ramjet (A2). In the ramjet case, the Mach number at the leading edge of the cavity is assumed to be that after a normal shock, corresponding to a local Mach number of 0.577 while T_{01} is the same owing to adiabatic flow. The solid lines are calculated by a simple heat release model with constant specific heat coefficient and no dissociation of the product species, while the dashed lines are assuming that the product mixture is in complete equilibrium and temperature dependency of full product mixture included in the analysis.

Considering the current maximum area ratio of the diverging section of the UVa combustor of 1.45 (horizontal dashed line), Fig. 33 shows the choking limit equivalence ratio at Mach 2 and 0.577 is 0.24 and 0.45, respectively. The experimental results from the UVa combustor have indicated limiting equivalence ratios of about 0.28 and 0.42 in close agreement with above phenomenological model. Furthermore, the above figure can be used to identify operability limits of UVa facility identified by the blue triangle, which is bounded by the flame holding conditions and non-choked operating conditions.

V. Conclusions

The National Center for Hypersonic Combined Cycle Propulsion was a 5-year research program. It was funded by NASA and AFOSR during years 1-3 and AFOSR during years 4 and 5.

In years 1-3, three facilities were used in the three combined cycle flow regimes. The IMX and LIMX facilities at NASA Glenn provided data to Boeing in the dual-inlet transition regime. The UVa dual-mode combustion facility was used for experiments in the dual-mode transition regime. The facility was operated in configurations A and C. The NASA HyPulse facility at ATK GASL provided data in the hypervelocity regime.

Extensive flow diagnostics were used in the UVa facility. This included SPIV (UVa), CARS and OH PLIF (GWU), TDLAS (Stanford) and TDLAT (UVa). TDLAS was used in the HyPulse facility.

Numerical modeling in years 1-3 included Generation I modeling at Boeing and NCSU, Generation II modeling at NCSU and MSU and Generation III modeling at U. Pittsburgh and U. Buffalo. A summary and overall appraisal of these numerical models was discussed.

Chemistry modeling in years 1-3 was done at UVa for model and flame extinction analysis and model reduction strategies. ISAT and RCCE models were developed at Cornell.

In years 4 and 5, the focus of the research was premixed flows. A Configuration E flowpath was developed at UVa. Extensive data was collected, to include pressure distributions, operability limits, chemiluminescence images and mode transition. Flow diagnostics in Configuration E included CARS, OH and NO PLIF by GWU, kHz PIV by UVa, and kHz PLIF by OSU. It was

demonstrated that the fuel injection scheme, using enhanced mixing by the isolator shock train, provided uniform premixed flow at the cavity entrance plane.

Numerical modeling in years 4 and 5 was done by NCSU and involved extensive LES/RANS nonreacting and reacting calculations of the UVa Configuration E. Chemistry modeling was done at UVa, to include ignition delay analysis and burning velocity calculations. A one-dimensional thermal choking model was developed for the Configuration E.

This Center provided the unique opportunity to bring together experts in experimentation and numerical modeling and chemistry modeling to focus on problems in hypersonic combined cycle propulsion. The data generated and the numerical and chemistry models developed establish a fundamental basis for the future development of propulsion systems of interest to the Air Force and NASA.

VI. Students and Post Doctoral Fellows Supported

The table below shows the students that were supported by the Center. Only the students at UVa, GWU and NCSU continued in years 4 and 5.

| Institution | PhD | MS | Post Doc |
|--------------------|------------|-----------|-----------------|
| U. Virginia | 9 | 1 | 2 |
| U. Pittsburgh | 3 | 0 | 1 |
| U. Buffalo | 2 | 0 | 0 |
| Cornell | 1 | 0 | 2 |
| George Wash U. | 3 | 0 | 0 |
| Michigan SU | 2 | 0 | 2 |
| Boeing | 1 | 0 | 0 |
| North Carolina SU | 2 | 1 | 1 |
| Stanford | 3 | 0 | 0 |
| Totals | 26 | 2 | 8 |

VII. Invited Special Session and Publications

AIAA Scitech 2015 (53rd AIAA Aerospace Sciences Meeting) Invited Session: Premixed High Speed Combustion

1. Robert D. Rockwell, Christopher P. Goyne, Brian Rice, Harsha K. Chelliah, James C. McDaniel, Jack R. Edwards, Luca Cantu, Emanuela Gallo, Andrew D. Cutler, Paul M. Danehy, "Development of a Premixed Combustion Capability for Dual-Mode Scramjet Experiments," AIAA 2015-0353
2. Harsha Chelliah, "Thermal and Chemical Kinetic Analysis of a High-Speed Reacting Flow in a Variable Area Duct," (Oral presentation)
3. Luca Cantu, Emanuela Gallo, Andrew D. Cutler, Brett F. Bathel, Paul M. Danehy, Robert D. Rockwell, Christopher P. Goyne, James C. McDaniel, "Nitric Oxide PLIF Visualization of Simulated Fuel-Air Mixing in a Dual-Mode Scramjet," AIAA 2015-0354
4. Andrew Cutler, "Coherent Anti-Stokes Raman Spectroscopy (CARS) in a Dual-Mode Scramjet with Premixed Fueling," (Oral Presentation) – see also Gallo E.C.A., Cantu, L.M.L., Cutler, A.D., Rahimi, M.J., Chelliah, H.K., "WIDECARS Measurements of Major Species Concentration and Temperature in an Air-Ethylene Flame," AIAA-2014-2525, AIAA Aviation and Aeronautics Forum and Exposition (AVIATION 2014) Atlanta, GA, 16 - 20 Jun 2014
5. Justin W. Kirik, Christopher P. Goyne, James C. McDaniel, Robert D. Rockwell, Ryan F. Johnson, Harsha K. Chelliah, "Velocimetry Using Graphite Tracer Particles in a Scramjet Flowpath," AIAA 2015-0355
6. Kiran Kumar Ramesh, Jack R. Edwards, Christopher P. Goyne, James C. McDaniel, "Large Eddy Simulation of High-Speed, Premixed Ethylene Combustion," AIAA 2015-0356
7. Kristin M. Busa, Brian Rice, James C. McDaniel, Christopher P. Goyne, Robert D. Rockwell, Jesse A. Fulton, Jack R. Edwards, Glenn S. Diskin, "Direct Measurement of Combustion Efficiency of a Dual-Mode Scramjet via TDLAT and SPIV," AIAA 2015-0357

Journal articles published by Center

2015

1. Cutler, A.D., Cantu, L.M.L., Gallo, E.C.A., Baurle, R., Danehy, P.M., Rockwell, R., Goyne, C., McDaniel, J.C., "Nonequilibrium Supersonic Freestream Studied Using Coherent Anti-Stokes Raman Spectroscopy," **AIAA J.**, published online, 2015: doi: 10.2514/1.J053748

2014

1. G Esposito, MJ Rahimi , HK Chelliah, PD Vogel, J. Edwards, "Assessment of Chemical Kinetic Modeling for Silane/Hydrogen Mixtures in Hypersonic Applications," **AIAA Journal**, **52**(10), 2014.
2. Johansen, C.T., McRae, C.D, Danehy, P.M, Gallo, E.C.A., Cantu, L.M.L, Magnotti, G, Cutler, A.D, Rockwell Jr., R.D., Goyne, C.P, McDaniel, J.C, "OH PLIF visualization of the UVa supersonic combustion experiment: configuration A," **J Vis** (2014) 17:131–141
3. Cutler, A.D., Magnotti, G., Cantu, L., Gallo, E., Rockwell, R.D., Goyne, C.P., "Coherent Anti-Stokes Raman Spectroscopy Measurements in a Dual-Mode Scramjet," **Journal of Propulsion and Power**, Vol. 30, Issue 3, pp. 539-549 (2014)
4. Fulton, J.A., Edwards, J.R., Hassan, H.A., McDaniel, J.C., Goyne, C.P., Rockwell, R.D., Cutler, A.D., Johansen, C.T., Danehy, P.M., "Large-Eddy/Reynolds-Averaged Navier–Stokes Simulations of Reactive Flow in Dual-Mode Scramjet Combustor," **Journal of Propulsion and Power**, 2014, Vol.30: 558-575
5. Amarnatha S. Potturi, Jack R. Edwards, "Hybrid Large-Eddy/Reynolds-Averaged Navier–Stokes Simulations of Flow Through a Model Scramjet," **AIAA Journal**, 2014, Vol.52: 1417-1429
6. Ian A. Schultz, Christopher S. Goldenstein, Jay B. Jeffries, Ronald K. Hanson, Robert D. Rockwell, Christopher P. Goyne , "Diode Laser Absorption Sensor for Combustion Progress in a Model Scramjet," **Journal of Propulsion and Power**, 2014, Vol.30: 550-557.
7. Ian A. Schultz, Christopher S. Goldenstein, Jay B. Jeffries, Ronald K. Hanson, Robert D. Rockwell, Christopher P. Goyne, "Spatially Resolved Water Measurements in a Scramjet Combustor Using Diode Laser Absorption," **Journal of Propulsion and Power**, 2014, Vol.30: 1551-1558
8. Ian A. Schultz, Christopher S. Goldenstein, R. Mitchell Spearrin, Jay B. Jeffries, Ronald K. Hanson, Robert D. Rockwell, Christopher P. Goyne, "Multispecies Midinfrared Absorption Measurements in a Hydrocarbon-Fueled Scramjet Combustor," **Journal of Propulsion and Power**, 2014, Vol.30: 1595-1604
9. Robert D. Rockwell Jr., Christopher P. Goyne, Brian E. Rice, Toshinori Kouchi, James C. McDaniel, Jack R. Edwards, "Collaborative Experimental and Computational Study of a Dual-Mode Scramjet Combustor," **Journal of Propulsion and Power**, 2014, Vol.30: 530-538
10. P.P. Popov, S.B. Pope, "Implicit and explicit schemes for mass consistency preservation in hybrid particle/finite-volume algorithms for turbulent reactive flows," **Journal of Computational Physics** (2014), 257, 352-373.

2013

1. Magnotti, G., Cutler, A.D., Danehy, P.M., "Development of a Dual-Pump CARS System for Measurements in Supersonic Combustion," **Applied Optics**, Vol. 52, Issue 20, pp. 4779-4791 (2013).
2. V. Hiremath, S.R. Lantz, H. Wang and S.B. Pope, "Large-scale Parallel Simulations of Turbulent Combustion Using Combined Dimension Reduction and Tabulation of Chemistry," **Proceedings of the Combustion Institute**, 205-215 (2013).

3. S.B. Pope, "Small scales, many species and the manifold challenges of turbulent combustion," **Proceedings of the Combustion Institute**, 1-31 (2013).
4. C.S. Goldenstein, J.B. Jeffries, R.K. Hanson, "Diode-laser measurements of linestrength and temperature-dependent lineshape parameters of H₂O, CO₂, and N₂-perturbed H₂O transitions near 2474 and 2482nm," **Journal of Quantitative Spectroscopy and Radiative Transfer** 2013; 130: 100-111.
5. C.S. Goldenstein, I.A. Schultz, J. B. Jeffries, R.K. Hanson, A two-color absorption spectroscopy strategy for measuring column density and path-average temperature in nonuniform gases," **Applied Optics**, 2013; 52: 7950-7962.
6. Benjamin J. Tatman, Robert D. Rockwell, Chris P. Goyne, James C. McDaniel, James M. Donohue, "Experimental Study of Vitiation Effects on Flameholding in a Cavity Flameholder," **Journal of Propulsion and Power**, 2013, Vol.29: 417-423
7. V. Hiremath, S. R. Lantz, H. Wang, and S. B. Pope, "Large-Scale Parallel Simulations of Turbulent Combustion using Combined Dimension Reduction and Tabulation of Chemistry," **Proceedings of the Combustion Institute**, 34, 205–215 (2013).

2012

1. V. Hiremath, S.R. Lantz, H. Wang, S.B. Pope, "Computationally-efficient and scalable parallel implementation of chemistry in simulations of turbulent combustion," **Combustion and Flame**, 159(12), 3096-3109, 2012.
2. Marrocco , M., Magnotti , G., Cutler, A.D., "Herman-Wallis Corrections in Dual-Pump CAR Intensities for Combustion, Temperature and Species," **Journal of Raman Spectroscopy**, Vol. 43, Issue 5, May 2012, pp. 595–598.
3. Magnotti, G., Cutler, A.D., Herring, G.C., Tedder, S.A., Danehy, P.M., "Saturation and Stark Broadening Effects in Dual-Pump CARS of N₂, O₂ and H₂," **Journal of Raman Spectroscopy**, Vol. 43, Issue 5, May 2012, pp. 611–620.
4. Cutler, A.D., Magnotti, G., "CARS Spectral Fitting with Multiple Resonant Species Using Sparse Libraries," **Journal of Raman Spectroscopy**, Vol. 42, Issue 11, 2011, pp. 1949-1957.
5. R. Rockwell, C.P. Goyne, W.L. Haw, J.C. McDaniel, C.S. Goldenstein, I.A. Schultz, J.B. Jeffries, R.K. Hanson, "Measurement of water vapor levels for investigation of test gas vitiation effects on scramjet performance," **Journal of Propulsion and Power** 27 (2011) 1315-1317.
6. Sarnacki, B.G., Esposito, G., Krauss, R.H. and Chelliah, H.K., "Extinction Limits and Associated Uncertainties of Non-Premixed Counterflow Flames of Methane, Ethylene, Propylene and n-Butane in Air, **Combustion and Flame**," **Combustion and Flame** 159, 1026–1043, 2012.
7. Edwards, J.R., Boles, J.A., and Baurle, R.A. "Large-Eddy / Reynolds-Averaged Navier-Stokes Simulation of a Supersonic Reacting Wall Jet" **Combustion & Flame**, Vol. 159, No. 3, 2012, pp. 1127-1138.
8. Magnotti, G., Cutler, A.D., Danehy, P.M., "Beam Shaping for CARS Measurements in Turbulent Environments," **Applied Optics**, Vol. 51, Issue 20, 2012, pp. 4730-4741.
9. Z. Li, and F.A. Jaber, "A High-Order Finite-Difference Method for Numerical Simulations of Supersonic Turbulent Flows," **International Journal of Numerical Methods in Fluids**, pp. 740–766, Volume 68(6), 2012.

10. Esposito, G and Chelliah, HK, "Uncertainty, propagation of Chemical Kinetic Parameters and Binary Diffusion Coefficients in Predicting Extinction Limits of Hydrogen/Oxygen/Nitrogen Nonpremixed Flames" I, **Combustion Theory and Modelling**, 16, 1029-1052 (2012)
11. N. Ansari, P.H. Pisciuneri, P.A. Strakey and P. Givi, "Scalar-Filtered Mass-Density-Function Simulation of Swirling Reacting Flows on Unstructured Grid, **AIAA Journal**, 2012, Vol.50: 2476-2482
12. Esposito, G and Chelliah, HK, "Effect of Binary Diffusion and Chemical Kinetic Parameters Uncertainties in Premixed and Non-premixed Laminar Hydrogen Flames," **Combustion and Flame**, 59, 3522–3529 (2012).
13. Edwards, J.R., Boles, J.A., and Baurle, R.A. "Large-Eddy / Reynolds-Averaged Navier-Stokes Simulation of a Supersonic Reacting Wall Jet" **Combustion & Flame**, Vol. 159, No. 3, 2012, pp. 1127-1138 (2012).
14. K. A. Kemenov, H. Wang, S. B. Pope, "Modeling effects of subgrid-scale mixture fraction variance in LES of a piloted diffusion flame," **Combustion Theory and Modelling**, 16(4), 611-638 (2012).

2011: Published

1. Ren, Z. Goldin, G.M. Hiremath, V. and Pope, S.B., "Reduced Description of Reactive Flows with Tabulation of Chemistry," **Combustion Theory and Modelling**, 15, 827-848, 2011.
2. Giesekeing, D.A., Choi, J.I., Edwards, J.R. and Hassan, H.A., "Compressible Flow Simulation using a New Large-Eddy Simulation/Reynolds-Averaged Navier Stokes Model," **AIAA Journal**, Vol. 49, No. 10, 2011. pp. 2194-2209.
3. N. Ansari, G.M. Goldin, M.R.H. Sheikhi, and P. Givi., "Filtered Density Function Simulator on Unstructured Meshes, **Journal of Computational Physics**, 230, pp. 7132-7150.
4. Noda, J, Tomioka, S, Izumikawa, M, Goyne, CP, Rockwell, RD, and Masuya, G, "Estimation of Enthalpy Effects in Direct-Connect Dual-mode Combustor," **Journal of Thermal Science and Technology**, Vol 6, No 2, 2011.
5. Smith, C, and Goyne, CP, "Application of Stereoscopic Particle Image Velocimetry to a Dual-mode Scramjet, **Journal of Propulsion and Power**, Vol 27, No 6, 2011, pp. 1178-1185.
6. Li, Z. and Jaber, F.A., "A High-Order Finite-Difference Method for Numerical Simulations of Supersonic Turbulent Flows," **International Journal of Numerical Methods in Fluids**, pp. 740–766, Volume 68(6), 2011.
7. Ansari, N., Goldin, G.M., Sheikhi, M.R.H. and Givi, P., "Filtered Density Function Simulator on Unstructured Meshes," **Journal of Computational Physics**, Vol. 230, 2011, pp. 7132-7150.
8. Yilmaz, S.L., Nik, M.B., Sheikhi, M.R.H., Strakey, P.A. and Givi, P., "An Irregularly Portioned Lagrangian Monte Carlo Method for Turbulent Flow Simulation," **Journal of Scientific Computation**, Vol. 47, No. 1, 2011, pp. 109-125.
9. Giesekeing, D.A., Choi, J.I., Edwards, J.R. and Hassan, H.A., "Compressible Flow Simulation using a New Large-Eddy Simulation/Reynolds-Averaged Navier Stokes Model," **AIAA Journal**, Vol. 49, No. 10, 2011. pp. 2194-2209.

10. Hiremath, V., Ren, Z. and Pope, S.B., "Combined Dimension Reduction and Tabulation Strategy using ISAT-RCCE-GALI for the Efficient Implementation of Combustion Chemistry", **Combustion and Flame**, 158(11) 2113-2127, 2011.
11. Rockwell, R.D., Goyne, C.P., Haw, W.L., Krauss, R.H., McDaniel, J.C. and Trefny, C.J., "Experimental Study of the Effects of Test Media Vitiating on the Performance and Operation of a Dual-Mode Scramjet," **Journal of Propulsion and Power**, Vol. 27, No. 5, pp.1135-1142, 2011.
12. Esposito, G., Chelliah, HK, "Skeletal reaction models based on principal component analysis: Application to ethylene-air ignition, propagation, and extinction phenomena," **Combustion and Flame**, 158, 2011, pp. 477-489.
13. Haw, W. L., Goyne, C. P., Rockwell, R. D., Krauss, R. H., and McDaniel, J. C., "Experimental Study of Vitiating Effects on Scramjet Mode Transition," **Journal of Propulsion and Power**, Vol. 27, No. 2, 2011, pp.506-508.
14. Rockwell, R. D., Goyne, C. P., Haw, W., McDaniel, J. C., Goldenstein, C. S., Schultz, I. A., Jeffries, J. B, and Hanson, R. K., "Measurement of Water Vapor Levels for Investigating Vitiating Effects on Scramjet Performance," **Journal of Propulsion and Power**, Vol. 27, No. 6, pp. 1315-1317, 2011.
15. Banaeizadeh, A., Li, Z., and Jaber, F.A., "Compressible Scalar FMDF Model for Large-Eddy Simulations of High speed Turbulent Flows," **AIAA Journal**, 49(10):2130-2143, 2011.
16. Hanson, R.K., "Applications of quantitative laser sensors to kinetics, propulsion, and practical energy systems," **Proceedings Combustion Institute** 33, 2011, pp. 1-40.
17. K. A. Kemenov, H. Wang , S. B. Pope, "Turbulence Resolution Scale Dependence in Large-Eddy Simulation of a Jet Flame," **Flow, Turbulence and Combustion** (2011).

2010: Published

1. Pope, S.B., "Self-Conditioned Fields for Large-Eddy Simulation of Turbulent Flows," **Journal of Fluid Mechanics**, Vol. 652, 2010, pp. 139-169.
2. Hiremath, V., Ren, Z. and Pope, S.B., "A Greedy Algorithm for Species Selection in Dimension Reduction of Combustion," **Combustion Theory and Modelling**, Vol. 14 (5) 2010, pp. 619-652.
3. Tedder, S.A., Wheeler, J.L., Cutler, A.D., Danehy, P.M., "Width-Increased Dual-Pump Enhanced Coherent Anti-Stokes Raman Spectroscopy (WIDECARS)," **Applied Optics** Vol. 49, Iss. 8, 2010, pp. 1305-1313.
4. Yaldizli, M., Mehravaran, K., Jaber, F.A., "Large-Eddy Simulations of Turbulent Methane Jet Flames with Filtered Mass Density Function," **International Journal of Heat and Mass Transfer**, 53, 2010, pp. 2551-2562.
5. Howison, J. and Goyne, C.P., "Assessment of Seeder Performance for Particle Velocimetry in a Scramjet Combustor," **Journal of Propulsion and Power**, Vol 26, No 3, 2010, pp. 514-523.
6. Ghosh, S., Choi, J.I. and Edwards, J.R., "Simulation of Shock/Boundary-Layer Interaction with Bleed using Immersed Boundary Methods," **Journal of Propulsion and Power**, Vol. 26, No. 2, 2010, pp. 203-214.

7. Martin, E.F., Goyne, C.P. and Diskin, G.S., "Analysis of a Tomography Technique for a Scramjet Wind tunnel," **International Journal of Hypersonics**, Vol. 1, No. 3, 2010, pp. 173-180.
8. Boles, J.A., Edwards, J.R. and Baurle, R.A., "Large-Eddy/Reynolds-Averaged Navier Stokes Simulations of Sonic Injection into a Mach 2 Crossflow," **AIAA Journal**, Vol. 48, No. 7, 2010, pp. 1444-1456.
9. Nik, M.B., Yilmaz, S.L., Sheikhi, M.R.H. and Givi, P., "Grid Resolution Effects on VSFMD/LES," **Flow in Turbulent Combustion**, Vol. 85, No. 3-4, 2010, pp. 677-688.

1.

1. Report Type

Final Report

Primary Contact E-mail

Contact email if there is a problem with the report.

jcm@virginia.edu

Primary Contact Phone Number

Contact phone number if there is a problem with the report

434-924-6293

Organization / Institution name

University of Virginia

Grant/Contract Title

The full title of the funded effort.

National Center for Combined Cycle Propulsion

Grant/Contract Number

AFOSR assigned control number. It must begin with "FA9550" or "F49620" or "FA2386".

FA9550-09-1-0611

Principal Investigator Name

The full name of the principal investigator on the grant or contract.

James C. McDaniel, Jr.

Program Manager

The AFOSR Program Manager currently assigned to the award

Chiping Li

Reporting Period Start Date

06/01/2009

Reporting Period End Date

12/31/2014

Abstract

The National Center for Hypersonic Combined Cycle Propulsion was a 5-year Center of Excellence in Hypersonics funded by the Air Force Office of Scientific Research and NASA. The Center utilized experts in experimentation and numerical and chemical modeling to address the flow physics in the combined cycle. It was found that, using RANS models, in the turbine/ramjet dual-inlet transition, the properties at the turbine inlet plane were determined by the shock/turbulent boundary layer interaction at the bleed ports and that the ports could be modeled with a surface bleed pattern model, without the need to model the bleed reservoirs. Dual-mode combustion wind tunnels were developed for studying the ramjet/scramjet mode transition. It was found that, with an isolator, the mode remained supersonic (scramjet) for equivalence ratios below 0.38; at higher equivalence ratios, a pre-combustion shock train was established in the isolator, causing the flow to become subsonic (ramjet) in a one-dimensional sense. Stereoscopic particle image velocimetry demonstrated that the streamwise vortices generated by a ramp fuel injector dominate the flow mixing in the supersonic mode, but with the pre-combustion shock train in the dual mode regime they are much weaker and the subsonic

DISTRIBUTION A: Distribution approved for public release.

flow is then dominated by the high momentum of the fuel jet. Coherent Anti-stokes Raman Scattering detected vibrational non-equilibrium for the inflow to the dual-mode combustor, which was included in numerical models. Using a column density approach, TDLAS measurements of water vapor and temperature were made while being insensitive to flow density variation along the optical path. TDLAT and SPIV measurements were combined to measure combustion efficiency. It was found that the combustion efficiency was higher when the flow was in the ram mode versus the scram mode. In the NASA HyPulse pulsed shock facility it was shown that the flow at Mach 7 enthalpy was not well suited to stable flameholding at the low temperatures without the addition of a silane additive. RANS models were also found to be inadequate due to the lack of existing silane kinetic models at low temperature. LES/RANS models were applied to the complex reactive flows and were found to be in excellent agreement with measurements in the dual-mode regime. A strained laminar flamelet theory showed that the vortices shed by the ramp fuel injector enhance mixing, but lead to very high local strain rates in parts of the flame, causing regions of local extinction. Flame stabilization occurs in the low-momentum region at the base of the flameholder where strain rates are lower and residence times are higher. FDF methods using a Lagrangian particle-based approach were shown to have the advantage that subgrid-scale effects of turbulence on reaction source terms can be represented in closed form. Improved ways were developed to couple the particle methods with Eulerian solvers to predict the correct pressure jump through shock waves. An energy-pressure-frequency-velocity-scalar (EPFVS) FDF was developed and revealed major challenges in closing various terms in the stochastic equations for energy and pressure. A domain decomposition method was developed for the ensemble of FDF notional particles, termed the 'irregular portioning method,' which allowed the particle-based solver to be ported to thousands of CPU cores. DNS simulations of canonical compressible turbulent flows were conducted in an attempt to provide data suitable for FDF model development. Using a flame extinction analysis, it was shown that the molecular transport coefficient uncertainties are of the same order as the counterflow extinction limit measurement uncertainties, while the chemical kinetic model uncertainties are much greater than the experiments. Chemical kinetic model reduction strategies were developed using skeletal reaction models and rate-controlled constrained equilibrium (RCCE) with in-situ adaptive tabulation (ISAT) to reduce the number of represented species required in the kinetic models. In premixed flows in the compressible, turbulent regime, it was demonstrated, both experimentally and numerically, that the flow at a cavity flameholder entry plane could be well premixed using isolator fuel injection and the pre-combustion shock train in the dual-mode regime, but not in the scramjet regime. Lean and low temperature flameout experiments established the operability of the cavity flameholder with premixed in-flow of ethylene/air. Chemiluminescence imaging and numerical models revealed the structure of the flame. It was found that classical turbulent flame-speed estimates, using Zimont's model, produced favorable comparisons with measured flame angles. The most probable cavity residence time was calculated to be about 10 ms for the dual mode case and 2.5 ms in the supersonic mode. This is why dual-mode operation is favorable for flame stabilization. NO PLIF demonstrated the high degree of premixing at the cavity entrance plane. Extensive CARS measurements were made at the end of the Center in the premixed, cavity-stabilized flow and will be analyzed in the future. OH PLIF measurements showed that the flame from the cavity is two-dimensional, with only minor side-wall effects, and that the flame angle varies little with equivalence ratio and stagnation temperature. The flame propagation angle appears to be dependent primarily on the diffusion of radicals and energy across the cavity shear layer by preexisting inflow freestream turbulence. A technique using graphite flakes was developed to conduct PIV imaging with minimal particle fouling of the tunnel windows. Ignition delay calculations in the premixed Mach 2 flow, with static temperature of 677K and static pressure of 0.3 atm,

showed that the kinetic delay time was of order 100 sec, far exceeding the local main flow residence time of about 0.2 msec, confirming the need for the flame stabilizing mechanism of the cavity. It was found that a 1-5% mass exchange rate between the cavity and the main flow reduced the ignition delay time to 0.2 msec, the same as the main flow residence time. A quasi-one-dimensional thermal choking analysis predicted the thermal choking limits of the premixed flow in both the dual-mode and the supersonic mode. Dissociation was shown to have minimal effect on the thermal choking limits in the low equivalent ratios available in the dual-mode facility at 1200K stagnation temperature. Extensive observations of the fundamental physics of the complex combined cycle flowfield were well documented in the numerous publications by Center investigators.

Distribution Statement

This is block 12 on the SF298 form.

Distribution A - Approved for Public Release

Explanation for Distribution Statement

If this is not approved for public release, please provide a short explanation. E.g., contains proprietary information.

SF298 Form

Please attach your SF298 form. A blank SF298 can be found [here](#). Please do not password protect or secure the PDF. The maximum file size for an SF298 is 50MB.

[SF 298 - 2.pdf](#)

Upload the Report Document. File must be a PDF. Please do not password protect or secure the PDF. The maximum file size for the Report Document is 50MB.

[final, final report.pdf](#)

Upload a Report Document, if any. The maximum file size for the Report Document is 50MB.

Archival Publications (published) during reporting period:

2015

1. Cutler, A.D., Cantu, L.M.L., Gallo, E.C.A., Baurle, R., Danehy, P.M., Rockwell, R., Goyne, C., McDaniel, J.C., "Nonequilibrium Supersonic Freestream Studied Using Coherent Anti-Stokes Raman Spectroscopy," AIAA J., published online, 2015: doi: 10.2514/1.J053748

2014

1. G Esposito, MJ Rahimi , HK Chelliah, PD Vogel, J. Edwards, "Assessment of Chemical Kinetic Modeling for Silane/Hydrogen Mixtures in Hypersonic Applications," AIAA Journal, 52(10), 2014.
 2. Johansen, C.T., McRae, C.D, Danehy, P.M, Gallo, E.C.A., Cantu, L.M.L, Magnotti, G, Cutler, A.D, Rockwell Jr., R.D., Goyne, C.P, McDaniel, J.C, "OH PLIF visualization of the UVa supersonic combustion experiment: configuration A," J Vis (2014) 17:131–141
 3. Cutler, A.D., Magnotti, G., Cantu, L., Gallo, E., Rockwell, R.D., Goyne, C.P., "Coherent Anti-Stokes Raman Spectroscopy Measurements in a Dual-Mode Scramjet," Journal of Propulsion and Power, Vol. 30, Issue 3, pp. 539-549 (2014)
 4. Fulton, J.A., Edwards, J.R., Hassan, H.A., McDaniel, J.C., Goyne, C.P., Rockwell, R.D., Cutler, A.D., Johansen, C.T., Danehy, P.M., "Large-Eddy/Reynolds-Averaged Navier–Stokes Simulations of Reactive Flow in Dual-Mode Scramjet Combustor," Journal of Propulsion and Power, 2014, Vol.30: 558-575
 5. Amarnatha S. Potturi, Jack R. Edwards, "Hybrid Large-Eddy/Reynolds-Averaged Navier–Stokes Simulations of Flow Through a Model Scramjet," AIAA Journal, 2014, Vol.52: 1417-1429
 6. Ian A. Schultz, Christopher S. Goldenstein, Jay B. Jeffries, Ronald K. Hanson, Robert D. Rockwell, Christopher P. Goyne , "Diode Laser Absorption Sensor for Combustion
- DISTRIBUTION A: Distribution approved for public release.

Progress in a Model Scramjet," Journal of Propulsion and Power, 2014, Vol.30: 550-557.

7. Ian A. Schultz, Christopher S. Goldenstein, Jay B. Jeffries, Ronald K. Hanson, Robert D. Rockwell, Christopher P. Goyne, "Spatially Resolved Water Measurements in a Scramjet Combustor Using Diode Laser Absorption," Journal of Propulsion and Power, 2014, Vol.30: 1551-1558

8. Ian A. Schultz, Christopher S. Goldenstein, R. Mitchell Spearrin, Jay B. Jeffries, Ronald K. Hanson, Robert D. Rockwell, Christopher P. Goyne, "Multispecies Midinfrared Absorption Measurements in a Hydrocarbon-Fueled Scramjet Combustor," Journal of Propulsion and Power, 2014, Vol.30: 1595-1604

9. Robert D. Rockwell Jr., Christopher P. Goyne, Brian E. Rice, Toshinori Kouchi, James C. McDaniel, Jack R. Edwards, "Collaborative Experimental and Computational Study of a Dual-Mode Scramjet Combustor," Journal of Propulsion and Power, 2014, Vol.30: 530-538

10. P.P. Popov, S.B. Pope, "Implicit and explicit schemes for mass consistency preservation in hybrid particle/finite-volume algorithms for turbulent reactive flows," Journal of Computational Physics (2014), 257, 352-373.

2013

1. Magnotti, G., Cutler, A.D., Danehy, P.M., "Development of a Dual-Pump CARS System for Measurements in Supersonic Combustion," Applied Optics, Vol. 52, Issue 20, pp. 4779-4791 (2013).

2. V. Hiremath, S.R. Lantz, H. Wang and S.B. Pope, "Large-scale Parallel Simulations of Turbulent Combustion Using Combined Dimension Reduction and Tabulation of Chemistry," Proceedings of the Combustion Institute, 205-215 (2013).

3. S.B. Pope, "Small scales, many species and the manifold challenges of turbulent combustion," Proceedings of the Combustion Institute, 1-31 (2013).

4. C.S. Goldenstein, J.B. Jeffries, R.K. Hanson, "Diode-laser measurements of linestrength and temperature-dependent lineshape parameters of H₂O, CO₂, and N₂-perturbed H₂O transitions near 2474 and 2482nm," Journal of Quantitative Spectroscopy and Radiative Transfer 2013; 130: 100-111.

5. C.S. Goldenstein, I.A. Schultz, J. B. Jeffries, R.K. Hanson, A two-color absorption spectroscopy strategy for measuring column density and path-average temperature in nonuniform gases," Applied Optics, 2013; 52: 7950-7962.

6. Benjamin J. Tatman, Robert D. Rockwell, Chris P. Goyne, James C. McDaniel, James M. Donohue, "Experimental Study of Vitiating Effects on Flameholding in a Cavity Flameholder," Journal of Propulsion and Power, 2013, Vol.29: 417-423

7. V. Hiremath, S. R. Lantz, H. Wang, and S. B. Pope, "Large-Scale Parallel Simulations of Turbulent Combustion using Combined Dimension Reduction and Tabulation of Chemistry," Proceedings of the Combustion Institute, 34, 205-215 (2013).

2012

1. V. Hiremath, S.R. Lantz, H. Wang, S.B. Pope, "Computationally-efficient and scalable parallel implementation of chemistry in simulations of turbulent combustion," Combustion and Flame, 159(12), 3096-3109, 2012.

2. Marrocco, M., Magnotti, G., Cutler, A.D., "Herman-Wallis Corrections in Dual-Pump CARS Intensities for Combustion, Temperature and Species," Journal of Raman Spectroscopy, Vol. 43, Issue 5, May 2012, pp. 595-598.

3. Magnotti, G., Cutler, A.D., Herring, G.C., Tedder, S.A., Danehy, P.M., "Saturation and Stark Broadening Effects in Dual-Pump CARS of N₂, O₂ and H₂," Journal of Raman Spectroscopy, Vol. 43, Issue 5, May 2012, pp. 611-620.

4. Cutler, A.D., Magnotti, G., "CARS Spectral Fitting with Multiple Resonant Species Using Sparse Libraries," Journal of Raman Spectroscopy, Vol. 42, Issue 11, 2011, pp. 1949-1957.

5. R. Rockwell, C.P. Goyne, W.L. Haw, J.C. McDaniel, C.S. Goldenstein, I.A. Schultz, J.B.

Jeffries, R.K. Hanson, "Measurement of water vapor levels for investigation of test gas
DISTRIBUTION A: Distribution approved for public release.

- vitiation effects on scramjet performance," *Journal of Propulsion and Power* 27 (2011) 1315-1317.
6. Sarnacki, B.G., Esposito, G., Krauss, R.H. and Chelliah, H.K., "Extinction Limits and Associated Uncertainties of Non-Premixed Counterflow Flames of Methane, Ethylene, Propylene and n-Butane in Air, *Combustion and Flame*, Vol. 159, 1026–1043, 2012.
 7. Edwards, J.R., Boles, J.A., and Baurle, R.A. "Large-Eddy / Reynolds-Averaged Navier-Stokes Simulation of a Supersonic Reacting Wall Jet" *Combustion & Flame*, Vol. 159, No. 3, 2012, pp. 1127-1138.
 8. Magnotti, G., Cutler, A.D., Danehy, P.M., "Beam Shaping for CARS Measurements in Turbulent Environments," *Applied Optics*, Vol. 51, Issue 20, 2012, pp. 4730-4741.
 9. Z. Li, and F.A. Jaber, "A High-Order Finite-Difference Method for Numerical Simulations of Supersonic Turbulent Flows," *International Journal of Numerical Methods in Fluids*, pp. 740–766, Volume 68(6), 2012.
 10. Esposito, G and Chelliah, HK, "Uncertainty, propagation of Chemical Kinetic Parameters and Binary Diffusion Coefficients in Predicting Extinction Limits of Hydrogen/Oxygen/Nitrogen Nonpremixed Flames" I, *Combustion Theory and Modelling*, 16, 1029-1052 (2012)
 11. N. Ansari, P.H. Pisciuneri, P.A. Strakey and P. Givi, "Scalar-Filtered Mass-Density-Function Simulation of Swirling Reacting Flows on Unstructured Grid, *AIAA Journal*, 2012, Vol.50: 2476-2482
 12. Esposito, G and Chelliah, HK, "Effect of Binary Diffusion and Chemical Kinetic Parameters Uncertainties in Premixed and Non-premixed Laminar Hydrogen Flames," *Combustion and Flame*, 59, 3522–3529 (2012).
 13. Edwards, J.R., Boles, J.A., and Baurle, R.A. "Large-Eddy / Reynolds-Averaged Navier-Stokes Simulation of a Supersonic Reacting Wall Jet" *Combustion & Flame*, Vol. 159, No. 3, 2012, pp. 1127-1138 (2012).
 14. K. A. Kemenov, H. Wang, S. B. Pope, "Modeling effects of subgrid-scale mixture fraction variance in LES of a piloted diffusion flame," *Combustion Theory and Modelling*, 16(4), 611-638 (2012).
- 2011: Published
1. Ren, Z. Goldin, G.M. Hiremath, V. and Pope, S.B., "Reduced Description of Reactive Flows with Tabulation of Chemistry," *Combustion Theory and Modelling*, 15, 827-848, 2011.
 2. Giesekeing, D.A., Choi, J.I., Edwards, J.R. and Hassan, H.A., "Compressible Flow Simulation using a New Large-Eddy Simulation/Reynolds-Averaged Navier Stokes Model," *AIAA Journal*, Vol. 49, No. 10, 2011. pp. 2194-2209.
 3. N. Ansari, G.M. Goldin, M.R.H. Sheikhi, and P. Givi., "Filtered Density Function Simulator on Unstructured Meshes, *Journal of Computational Physics*, 230, pp. 7132-7150.
 4. Noda, J, Tomioka, S, Izumikawa, M, Goyne, CP, Rockwell, RD, and Masuya, G, "Estimation of Enthalpy Effects in Direct-Connect Dual-mode Combustor," *Journal of Thermal Science and Technology*, Vol 6, No 2, 2011.
 5. Smith, C, and Goyne, CP, "Application of Stereoscopic Particle Image Velocimetry to a Dual-mode Scramjet, *Journal of Propulsion and Power*, Vol 27, No 6, 2011, pp. 1178-1185.
 6. Li, Z. and Jaber, F.A., "A High-Order Finite-Difference Method for Numerical Simulations of Supersonic Turbulent Flows," *International Journal of Numerical Methods in Fluids*, pp. 740–766, Volume 68(6), 2011.
 7. Ansari, N., Goldin, G.M., Sheikhi, M.R.H. and Givi, P., "Filtered Density Function Simulator on Unstructured Meshes," *Journal of Computational Physics*, Vol. 230, 2011, pp. 7132-7150.
 8. Yilmaz, S.I., Nik, M.B., Sheikhi, M.R.H., Strakey, P.A. and Givi, P., "An Irregularly

- Portioned Lagrangian Monte Carlo Method for Turbulent Flow Simulation,” *Journal of Scientific Computation*, Vol. 47, No. 1, 2011, pp. 109-125.
9. Gieseeking, D.A., Choi, J.I., Edwards, J.R. and Hassan, H.A., “Compressible Flow Simulation using a New Large-Eddy Simulation/Reynolds-Averaged Navier Stokes Model,” *AIAA Journal*, Vol. 49, No. 10, 2011. pp. 2194-2209.
 10. Hiremath, V., Ren, Z. and Pope, S.B., “Combined Dimension Reduction and Tabulation Strategy using ISAT-RCCE-GALI for the Efficient Implementation of Combustion Chemistry”, *Combustion and Flame*, 158(11) 2113-2127, 2011.
 11. Rockwell, R.D., Goyne, C.P., Haw, W.L., Krauss, R.H., McDaniel, J.C. and Trefny, C.J., “Experimental Study of the Effects of Test Media Vitiatio on the Performance and Operation of a Dual-Mode Scramjet,” *Journal of Propulsion and Power*, Vol. 27, No. 5, pp.1135-1142, 2011.
 12. Esposito, G., Chelliah, HK, “Skeletal reaction models based on principal component analysis: Application to ethylene–air ignition, propagation, and extinction phenomena,” *Combustion and Flame*, 158, 2011, pp. 477–489.
 13. Haw, W. L., Goyne, C. P., Rockwell, R. D., Krauss, R. H., and McDaniel, J. C., “Experimental Study of Vitiatio Effects on Scramjet Mode Transition,”*Journal of Propulsion and Power*, Vol. 27, No. 2, 2011 , pp.506-508.
 14. Rockwell, R. D., Goyne, C. P., Haw, W., McDaniel, J. C., Goldenstein, C. S., Schultz, I. A., Jeffries, J. B, and Hanson, R. K., "Measurement of Water Vapor Levels for Investigating Vitiatio Effects on Scramjet Performance," *Journal of Propulsion and Power*, Vol. 27, No. 6, pp. 1315-1317, 2011.
 15. Banaeizadeh, A., Li, Z., and Jaber, F.A., “Compressible Scalar FMDF Model for Large-Eddy Simulations of High speed Turbulent Flows,” *AIAA Journal*, 49(10):2130–2143, 2011.
 16. Hanson, R.K., “Applications of quantitative laser sensors to kinetics, propulsion, and practical energy systems,” *Proceedings Combustion Institute* 33, 2011, pp. 1-40.
 17. K. A. Kemenov, H. Wang , S. B. Pope, “Turbulence Resolution Scale Dependence in Large-Eddy Simulation of a Jet Flame,” *Flow, Turbulence and Combustion* (2011). 2010: Published
 1. Pope, S.B., “Self-Conditioned Fields for Large-Eddy Simulation of Turbulent Flows,” *Journal of Fluid Mechanics*, Vol. 652, 2010, pp. 139-169.
 2. Hiremath, V., Ren, Z. and Pope, S.B., “A Greedy Algorithm for Species Selection in Dimension Reduction of Combustion,” *Combustion Theory and Modelling*, Vol. 14 (5) 2010, pp. 619-652.
 3. Tedder, S.A., Wheeler, J.L., Cutler, A.D., Danehy, P.M., "Width-Increased Dual-Pump Enhanced Coherent Anti-Stokes Raman Spectroscopy (WIDECARS)," *Applied Optics* Vol. 49, Iss. 8, 2010, pp. 1305-1313.
 4. Yaldizli, M., Mehravaran, K., Jaber, F.A., “Large-Eddy Simulations of Turbulent Methane Jet Flames with Filtered Mass Density Function,” *International Journal of Heat and Mass Transfer*, 53, 2010, pp. 2551-2562.
 5. Howison, J. and Goyne, C.P., “Assessment of Seeder Performance for Particle Velocimetry in a Scramjet Combustor,” *Journal of Propulsion and Power*, Vol 26, No 3, 2010, pp. 514-523.
 6. Ghosh, S., Choi, J.I. and Edwards, J.R., “Simulation of Shock/Boundary-Layer Interaction with Bleed using Immersed Boundary Methods,” *Journal of Propulsion and Power*, Vol. 26, No. 2, 2010, pp. 203-214.
 7. Martin, E.F., Goyne, C.P. and Diskin, G.S., “Analysis of a Tomography Technique for a Scramjet Wind tunnel,” *International Journal of Hypersonics*, Vol. 1, No. 3, 2010, pp. 173-180.
 8. Boles, J.A., Edwards, J.R. and Baurle, R.A., “Large-Eddy/Reynolds-Averaged Navier Stokes Simulations of Sonic Injection into a Mach 2 Crossflow,” *AIAA Journal*, Vol. 48, No. 7, 2010, pp. 1444-1456.

9. Nik, M.B., Yilmaz, S.L., Sheikhi, M.R.H. and Givi, P., "Grid Resolution Effects on VSFMD/LES," Flow in Turbulent Combustion, Vol. 85, No. 3-4, 2010, pp. 677-688.

Changes in research objectives (if any):

Years 4 and 5 changed focus to premixed compressible turbulent flows.

Change in AFOSR Program Manager, if any:

Extensions granted or milestones slipped, if any:

Extension granted from 7/31/2014 to 12/31/2014

AFOSR LRIR Number

LRIR Title

Reporting Period

Laboratory Task Manager

Program Officer

Research Objectives

Technical Summary

Funding Summary by Cost Category (by FY, \$K)

| | Starting FY | FY+1 | FY+2 |
|----------------------|-------------|------|------|
| Salary | | | |
| Equipment/Facilities | | | |
| Supplies | | | |
| Total | | | |

Report Document

Report Document - Text Analysis

Report Document - Text Analysis

Appendix Documents

2. Thank You

E-mail user

Mar 23, 2015 19:18:34 Success: Email Sent to: jcm@virginia.edu